Environ Monit Assess (2025) 197:1072
https://doi.org/10.1007/s10661-025-14502-8

RESEARCH

# Continental maize mapping and distribution in Africa by integrating radar and optical imagery

**Nasser A. M. Abdelrahim · Shuanggen Jin**

Received: 18 June 2025 / Accepted: 11 August 2025


**Abstract** High-resolution, accurate mapping of crops is critical to enhance food security, resource efficiency, and policy effectiveness in agriculture across Africa, where maize remains a crucial staple crop. However, mosaic landscapes, common cloud cover, and scarce ground information have hindered large-area and field-level maize monitoring. This study presents a novel continent-wide framework for mapping maize cultivation across Africa for the 2023–2024 growing season at 10-m resolution using multi-temporal and multi-sensor remote sensing data. Our approach integrates Sentinel-1 SAR and Sentinel-2 optical imagery with the support of expert-validated pseudo-ground truth samples, region-based spectral-temporal signature analysis, and object-oriented segmentation through the Simple Non-Iterative Clustering (SNIC) algorithm. Maize classification was performed using a random forest model, which achieved an overall accuracy of 87.8% (kappa = 0.81), with regional performance of above 91% in Southern Africa. The harvested maize area in Africa was estimated to be 44.1 million hectares, with the largest share belonging to the West African region (31.4%). Model estimates showed strong alignment with national agricultural statistics (Pearson's $r = 0.88$ when compared to FAOSTAT-reported areas). The resulting maps capture spatial variability in yield, cropping intensity, and field size. This study delivers one of the most detailed, cross-validated maize maps across Africa and proposes a method suitable for operational crop monitoring and food system planning amid climate variability.

**Keywords** Maize · Crop mapping · High resolution · Random forest (RF) · Sentinel data · Africa

N. A. M. Abdelrahim (✉) · S. Jin
Shanghai Astronomical Observatory, Chinese Academy of Sciences, Shanghai 200030, China
e-mail: nasserahmed@shao.ac.cn

S. Jin
e-mail: sgjin@hpu.edu.cn

N. A. M. Abdelrahim
School of Astronomy and Space Science, University of Chinese Academy of Sciences, Beijing 100049, China

N. A. M. Abdelrahim
Civil Engineering Department, Faculty of Engineering, Sohag University, Sohag 82511, Egypt

S. Jin
School of Artificial Intelligence, Anhui University, Hefei 230601, China

S. Jin
School of Surveying and Land Information Engineering, Henan Polytechnic University, Jiaozuo 454003, China

## Introduction

Maize (*Zea mays* L.) is the most cultivated cereal crop throughout Africa, serving as the primary source

Published online: 01 September 2025

of caloric intake for millions and playing a crucial role in national food systems and economies (Erenstein et al., 2022; Kou et al., 2024). In most African nations, maize contributes over half of the total cereal output and is mainly produced under rainfed, smallholder-dominated systems, which are extremely responsive to climatic variability, input availability, and market volatility (Epule et al., 2022). Current and geospatially precise information on where and to what proportion maize is being produced is therefore of paramount importance, not only for farm planning and policy but also for food security monitoring, climate resilience, and humanitarian intervention (Hou et al., 2024). However, standard field-level maize mapping across the entire continent has not yet been achieved due to a synergy of intricate biophysical, technical, and institutional bottlenecks (Jombo & Elbasit, 2024).

The presence of high-resolution Earth observation (EO) satellites and cloud-based geospatial software presents a revolutionary option to fill these information gaps (Abdelrahim & Jin, 2025a; Amaral et al., 2024; Jin et al., 2022, 2024, and 2025). In particular, the European Space Agency's 10–20-m spatial resolution and regular revisit cycle of Sentinel-1 and Sentinel-2 missions present a synergistic combination of spectral, structural, and temporal information (Abdelrahim & Jin, 2025b; Abdi, 2020; Bhogapurapu et al., 2022). Sentinel-2's multispectral imagery is well adapted to tracking vegetation change and growth phenology, while Sentinel-1's SAR is handy to differentiate canopy structure and wetness and, importantly, still works under persistent cloud cover, which is a typical issue in tropical Africa (Chen et al., 2023; Di Tommaso et al., 2023). Together, these measurements provide a temporally rich and synergistic foundation for robust crop type classification. This capability has been validated by recent research, with studies achieving high classification accuracies of maize and other crops from machine learning algorithms trained from Sentinel time-series data (Forkuor et al., 2018; Choukri et al., 2024). Much of this research has stayed confined to specific country or sub-country contexts.

Historically, Africa's crop mapping relied on low-resolution sensor imagery like MODIS or AVHRR, which are adequate for tracking regional-scale phenology but not of spatial resolution to capture fragmented smallholder holdings or field-level heterogeneity (António et al., 2024; Azzari et al., 2021; Heiss et al., 2025; Jeffries et al., 2020). Landsat satellites (30 m) are a significant development since research such as Potapov et al. (2012) mapped agricultural expansion in the Democratic Republic of Congo, and Abubakar et al. (2020) used S1 and S2 data to map maize fields in Makarfi, Northern Nigeria. Despite such advances, frequent cloud cover and a 16-day revisit cycle restricted routine phenological monitoring, particularly for maize, a climate-sensitive crop (Deines et al., 2019). Forkuor et al. (2018) demonstrated Sentinel-2's usability for maize mapping in Burkina Faso, and Mashaba-Munghemezulu et al. (2021) used these methods in South African smallholder systems.

Although high-performance machine learning methods such as random forests and deep neural networks are increasingly used in agricultural remote sensing, their scalability across Africa's heterogeneous agricultural landscapes remains underexplored (Maponya et al., 2020; Prins & Van Niekerk, 2021; Zhang et al., 2016). A major limitation is the lack of reliable training data in many African countries, where field information is often outdated or unavailable, undermining supervised classification models depending on vast, well-labeled datasets (Lin et al., 2022; Wang et al., 2019; Wen et al., 2022). Recent improvements in pseudo-ground truth creation, where training data are derived by experienced visual interpretation of phenological patterns in high-resolution time-series images, offer a promising alternative solution, but such methods are as yet underutilized for large-area crop mapping (Jiang et al., 2025; Lin et al., 2022).

To address these challenges, this study presents a new, functional, and scalable system for high-resolution (10-m) maize mapping across Sub-Saharan Africa, integrating multi-sensor satellite images, advanced feature engineering, object-based classification, and pseudo-labeled training data. The strategy is designed to overcome key limitations identified in the literature, specifically (i) to develop a robust, scalable, and high-resolution (10-m) framework for continental maize mapping in Africa by integrating multi-temporal Sentinel-1 SAR and Sentinel-2 optical imagery; (ii) to enhance mapping accuracy and robustness across diverse agro-ecological zones through the incorporation of a phenological alignment approach and expert-validated pseudo-ground truth samples; and (iii) to

demonstrate the operational utility of the developed framework for informing food security, climate resilience, and sustainable agricultural planning across the African continent. At the core of this architecture are Sentinel-1 and Sentinel-2 time-series fusion, complemented with auxiliary data such as CHIRPS rainfall, MODIS land surface temperature (LST), and SRTM topography, in order to extract Sentinel-1/Sentinel-2 features with maize-specific phenological, structural, and textural features.

The novelty of this work lies in four interrelated areas. First, we apply a pseudo-labeling technique to expert-guided visual examination of time-series signatures of high geographic scope without relying on conventional field observations (Jiang et al., 2025; Lin et al., 2022). Second, we mitigate the effects of field-level heterogeneity by implementing a robust object-based classification system that classifies imagery into meaningful agricultural objects (Farrag et al., 2020; Gaber et al., 2021; Zhang et al., 2020). Third, we create a multi-sensor feature space that is tailored for African agricultural systems and includes spectral indices (e.g., NDVI, EVI), SAR backscatter statistics, textural data, and phenological metrics (Abdi, 2020; Chen et al., 2023; Di Tommaso et al., 2023). Fourth, we use two methods to validate the results: spatial comparisons with national and sub-national agricultural data from FAOSTAT and other datasets and object-based accuracy metrics obtained from independent validation sets (Amiri et al., 2021; Brown & Pervez, 2014; Pérez-Hoyos et al., 2017; Pervez & Brown, 2010).

By interfacing technical complexity with real-world use, this research not only offers a reproducible methodology but also a highly useful information product. Ultimately, this study supports the operational deployment of high-resolution crop monitoring systems across Africa to continue advocating for more responsive and resilient agricultural development policies. The rest of this paper consists of study areas and data in Sect. 2; Sect. 3 shows the methodology; Sect. 4 presents results and discussion; and finally, the conclusion is given in Sect. 5.

## Study areas and Data

### Study areas

This study covers the entire African continent (Fig. 1), spanning from the Mediterranean coastline in the north to the Cape of Good Hope in the south, and from the Atlantic Ocean in the west to the Indian Ocean in the east. Africa, which has over 1.4 billion people and an area of over 30 million $km^2$, is endowed with a highly diverse range of climates, ecosystems, and farming systems (Amazirh et al., 2023). The climate of the continent ranges from temperate zones in the south, tropical rainforests close to the equator, semi-arid savannas, and hyper-arid deserts towards the north. This spatial heterogeneity creates distinct rainfall, cropping, and drought risk patterns in Africa (FAO, 2022; Samasse et al., 2018).

Northern Africa is dominated by the Sahara Desert, which has scant rainfall, averaging less than 100 mm per year, and agriculture exists only in irrigated zones along the Nile and Mediterranean coastlines (Abdelhedi & Zouari, 2020). By way of contrast, the Sahelian belt just south of the Sahara is exposed to seasonal rains from June to September, which maintain millet, sorghum, and livestock pastoralism; however, this region is highly susceptible to drought and historically subjected to severe drought crises (Rhein & Jansesberger, 2024). Heading south, West Africa boasts a bimodal precipitation regime at the Gulf of Guinea, with annual precipitation ranging from 1200 to 2500 mm, favoring major crops like oil palm, cassava, and cocoa (Adaawen, 2021; Ayugi et al., 2022).

Central Africa, dominated by the Congo Basin, experiences heavy precipitation of over 2000 mm annually, supporting extensive tropical rainforests as well as subsistence cassava, plantain, and maize cultivation. It is more volatile in East Africa, particularly the Horn of Africa, where the bimodal rainy seasons, or the “long rains” and “short rains,” regulate agricultural calendars (Han et al., 2022). The nations, including Ethiopia, Kenya, and Somalia, are subject to recurrent droughts, which are exacerbated by climatic irregularities like ENSO and Indian Ocean Dipole phases (AghaKouchak, 2015). Lastly, the Southern Africa region has a unimodal summer rainfall season between November and March, with annual precipitation varying between 500 and 1200 mm, favoring the production of maize, soybean, and sugarcane. But this area has also suffered repeated meteorological droughts, as in the case of South Africa and Zimbabwe (Hao et al., 2020; Nash et al., 2019; Xiong et al., 2017b). Table 1 shows the climatic characteristics of each of the study regions.

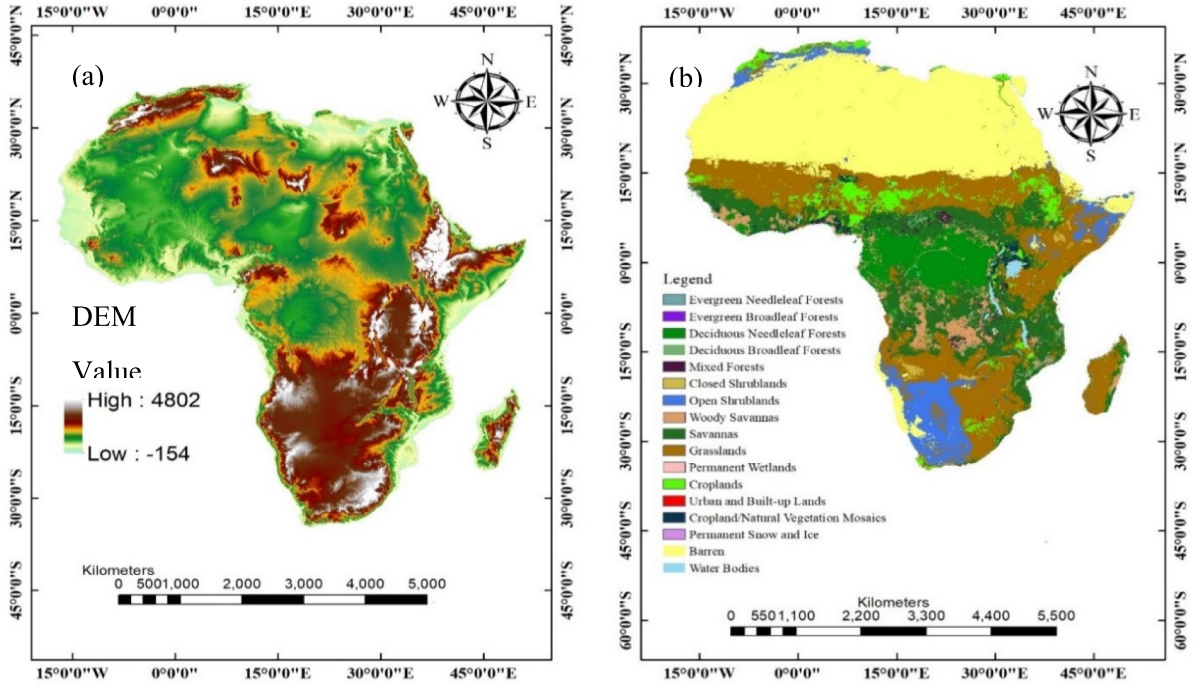


**Fig. 1** The map illustrates the African continent. **a** The topographic variation across Africa, emphasizing key regions such as the Ethiopian Highlands and the Congo Basin. **b** Land cover types (e.g., forests, savannas, deserts) derived from MODIS MCD12Q1 data

## Data acquisition

In order to represent maize distribution across Africa at 10-m resolution, this study integrates multi-sensor satellite observations and auxiliary topography and climate data. These data have been selected to identify maize's distinctive spectral, temporal, and structural characteristics to overcome issues such as cloud

**Table 1** Climatic and cropping characteristics of Africa's major regions

| Region | Climate type | Rainfall (mm/year) | Main crops | Drought vulnerability |
|---|---|---|---|---|
| North Africa | Arid to semi-arid (desert, Mediterranean along coast) | < 100 mm (Sahara), 200–600 mm (coastal) | Wheat, barley, olives, dates | High (chronic water scarcity, desertification) |
| Sahel (West Africa) | Semi-arid, monsoonal | 200–600 mm | Millet, sorghum, livestock | Very high (historic drought crises, e.g., 1980 s Sahel drought) |
| West Africa (Guinea Coast) | Humid tropical, bimodal rains | 1200–2500 mm | Cocoa, oil palm, cassava | Moderate (rainfall decline in recent decades) |
| Central Africa (Congo Basin) | Equatorial humid forest | 1500–2500 mm | Cassava, plantains, maize | Low (but vulnerable to short-term dry spells) |
| East Africa (Horn and Rift Valley) | Semi-arid to sub-humid, bimodal rains | 300–1200 mm | Maize, tea, coffee | Very high (frequent droughts, e.g., 2016–2017) |
| Southern Africa | Semi-arid to sub-humid, unimodal summer rains | 500–1200 mm | Maize, soybeans, sugarcane | High (recent severe droughts, e.g., 2015–2016 El Niño) |

cover, landscape heterogeneity, and limited ground truth.

Normalized Difference Vegetation Index (NDVI) was derived from Sentinel-2 (S2) Multispectral Instrument (MSI) Level-2A surface reflectance products (Furlanetto et al., 2023; Shao et al., 2021). With a spatial resolution of 10 m in the red-edge, near-infrared (NIR), and visible spectral bands, Sentinel-2 provides critical information on crop vigor and vegetation phenology (Di Tommaso et al., 2023). Monthly cloud-free NDVI composites were derived from Google Earth Engine (GEE) (Abubakar et al., 2023) by applying cloud masking with the QA60 band and the s2cloudless algorithm. NDVI is an important indicator of maize growth stages like green-up, maximum biomass, and senescence (Hao et al., 2016).

Synthetic aperture radar (SAR) backscatter measurements were retrieved from Sentinel-1 (S1) Ground Range Detected (GRD) products (C-band, VV/VH polarizations) (Chaudhary et al., 2022; Ouaadi et al., 2025). With a spatial resolution of 10 m and a revisit time of 6–12 days, Sentinel-1 offers frequent observation of vegetation structure and soil moisture changes, even under cloudy conditions (Gangat et al., 2020). Preprocessing consisted of biweekly median compositing, which was applied to reduce speckle noise; terrain correction using the Shuttle Radar Topography Mission (SRTM) Digital Elevation Model (DEM); and radiometric correction to sigma-nought ($\sigma^{\circ}$) (Mullissa et al., 2021).

To synchronize with Sentinel-2 images, the land surface temperature (LST) derived from MODIS MOD11A2 8-day composites was repatterned to a resolution of 10 m. In crop stress evaluation and discrimination among maize and non-crop vegetation, LST provides essential thermal information. In order to synchronize the time resolution of the other input variables, monthly aggregations were produced (Alexander, 2020; Khorrami & Gunduz, 2020).

Precipitation information was obtained from the Climate Hazards Group InfraRed Precipitation with Station (CHIRPS) dataset, integrating satellite retrievals and in situ station observations. CHIRPS rainfall records (0.05° spatial resolution) were resampled to 10 m and aggregated into monthly sums to assess moisture availability in maize growing periods (Khorrami et al., 2024).

Crop suitability and practice determining slope/aspect layers were created from the topography of the 30-m resolution SRTM DEM to normalize SAR backscatter for terrain effects (Gallant & Read, 2016; Xiong et al., 2017a).

HarvestChoice/IFPRI's CROPGRIDS maize production data at 10 km resolution provided subnational maize distribution patterns. The data were used as reference data for regional sampling design and validation rather than direct use in classification (Tang et al., 2024).

Reference data were created in the form of pseudo-ground truth samples using high-resolution imagery (0.5–1 m) taken from Google Earth and Bing Maps (Liu et al., 2020). Analysts used multi-temporal Sentinel-2 NDVI profiles and SAR backscatter trends and defined maize and non-maize polygons in a systematic manner, aided by visual cross-referencing with historical Google Earth imagery.

All datasets were harmonized into the WGS84 coordinate system and to a shared spatial grid (10 m) by nearest-neighbor resampling (Ghosh et al., 2024). Temporal harmonization was achieved by averaging Sentinel-1/2 and MODIS data to monthly composites to be compatible with maize phenological cycles. Table 2 describes the data characteristics.

## Methodology

This methodology leverages the multi-sensor fusion of S1 (SAR), S2 (optical), and ancillary data like MODIS, CHIRPS, and SRTM DEM within a machine learning framework. One of the major challenges in large-area crop mapping, particularly for heterogeneous African farming systems, is the scarcity of large and quality ground truth data for training classification models (Wang et al., 2019). To address this, the proposed method involves the generation of a robust pseudo-ground truth sample set (Deines et al., 2019). The process is structured into three main stages, as illustrated in Fig. 2: (1) pseudo-ground truth sample set construction, (2) image classification based on time-series features, and (3) map validation and refinement.

### Pseudo-ground truth sample set construction

The foundation of all supervised classification approaches is a precise and representative set of training data (Xiong et al., 2017a). Because of the

**Table 2** Datasets and remote sensing sources used for maize mapping

| Variable | Dataset | Spatial resolution | Temporal resolution | Period covered | Source |
|---|---|---|---|---|---|
| SAR backscatter (VV/VH) | Sentinel-1 GRD | 10 m | Bi-weekly/monthly | 2014–present | ESA Copernicus |
| Optical bands and NDVI | Sentinel-2 Level-2A | 10–20 m | Monthly | 2015–present | ESA Copernicus |
| Land surface temperature | MODIS MOD11A2 | 1 km → 10 m | Monthly | 2000–present | NASA LP DAAC |
| Precipitation | CHIRPS | 0.05° → 10 m | Monthly | 1981–present | CHIRPS Data Portal |
| Topography | SRTM DEM | 30 m | Static | 2000 | NASA SRTM |
| Regional crop reference | CROPGRIDS | 10 km | Annual | 2000–2015 | HarvestChoice/IFPRI |
| Pseudo-ground truth | Google Earth Imagery | 0.5–1 m | Historical | 2000–present | Google Earth Engine |

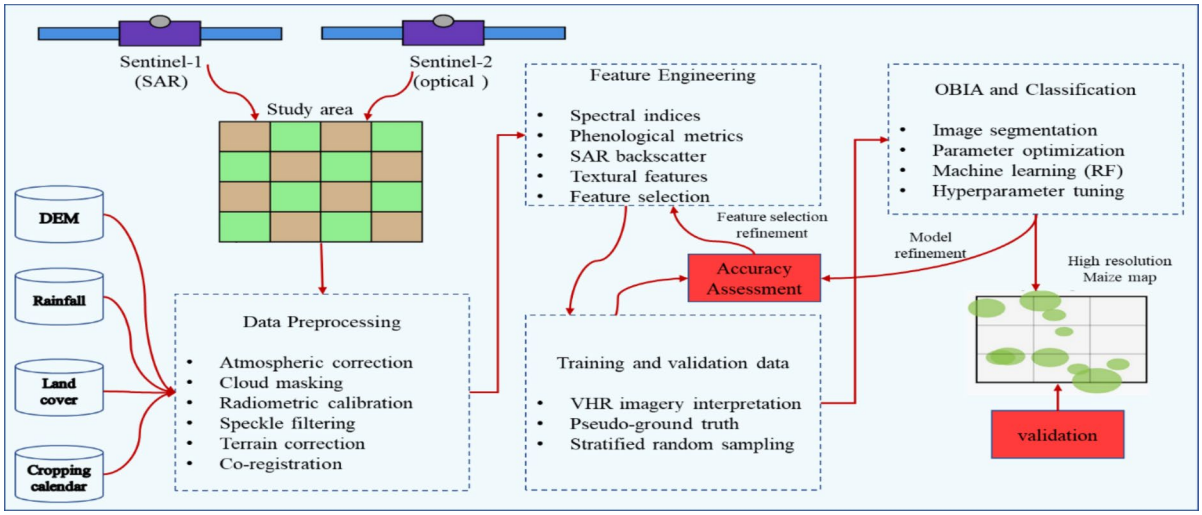


**Fig. 2** Overview of the methodological workflow

challenge of obtaining large-scale ground truth across Africa, this step involves the systematic development of pseudo-ground truth samples for "maize" and "non-maize" land cover classes (Lin et al., 2022). A total of 54 sub-regions were chosen to represent the variety of agricultural systems, agroclimatic variability, and rainfall patterns. Some of these sub-regions are semi-arid (like eastern Kenya), humid (like southern Nigeria), and irrigated (like the Nile Delta, Egypt). Within each, visual interpretation was conducted to delineate maize and non-maize fields based on temporally aligned NDVI and SAR backscatter profiles.

*Data preprocessing*

The primary satellite data sources are S1 SAR and S2 optical imagery. Preprocessing of S1 GRD products on GEE involves applying orbit files, removing thermal noise, radiometrically correcting backscatter coefficients ($\sigma^{\circ}$), and terrain correcting using SRTM DEM to prevent topographic distortion. Median monthly composites are generated to reduce speckle and enhance phenological consistency, where VH backscatter is extremely vulnerable to crop canopy growth (Mullissa et al., 2021).

S2 data are accessed at Level-2A (bottom-of-atmosphere reflectance) when available; otherwise, Level-1C data are corrected atmospherically by using software like Sen2Cor. Cloud and shadow masking is performed using the QA60 band or software like s2cloudless. From cloud-free optical mosaics, vegetation indices like NDVI are derived and temporally composited into monthly stacks to record phenological dynamics. NDVI, in particular, serves as the primary indicator of canopy development

and senescence, paramount in detecting crop cycles (Abdi, 2020).

Auxiliary data sets contain contextual information. MODIS products, such as LST (e.g., MOD11A1) and NPP (e.g., MOD17A3), provide thermal and productivity observations for use in distinguishing land covers and crop stress estimation. CHIRPS precipitation estimates, of almost global coverage at ~ 5 km resolution, are aggregated to monthly totals to represent climatic drivers of cropping calendars (Khorrami & Gunduz, 2020; Khorrami et al., 2024). SRTM DEM elevation and slope statistics are used both during SAR correction and as potential classification features. Finally, IFPRI CROPGRIDS data are used not for training input but as a spatial foundation to decipher sub-national trends of maize production, harvested area, and cropping intensity (Tang et al., 2024). These diverse datasets are spatially and temporally harmonized for subsequent feature extraction.

*Definition of maize and non-maize spectral-temporal signatures*

The identification of maize in satellite data is heavily reliant on characterizing its typical spectral and structural evolution throughout the growing season. Maize typically follows an orderly sequence of development: planting, vegetative growth, tasseling, grain filling, and senescence that is readily discernible in optical as well as radar observations (Collins et al., 2024). In Sentinel-2 NDVI time series, maize exhibits a sharp green-up immediately after planting, followed by a considerable NDVI peak during the flowering and grain-filling initiation phase (Bhatti et al., 2024; Brewer et al., 2022; Ni et al., 2022; Shuai et al., 2019). This is followed by a gradual decline as the crop enters senescence. The precise timing and magnitude of this NDVI peak, as well as the duration of the vegetative and reproductive phases, serve as critical indicators for maize identification, particularly when assessed over time.

Sentinel-1 SAR backscatter has the potential to make a major contribution to optical imagery by capturing canopy structural change over the course of a growing season. Early growth stages are characterized by low SAR backscatter, especially in VH polarization, due to minimal canopy volume and the predominance of soil signals. Greater crop development and biomass growth lead to increased VH backscatter levels with a peak at or near full canopy closure. This is succeeded by backscatter reduction following flowering, with correlating reductions in water content and subsequent revealing of the soil surface by harvest or senescence (Li et al., 2019). Interpreted jointly, radar and optical signals provide a robust temporal signature: for instance, a simultaneous increase in NDVI and VH backscatter represents healthy canopy development, characteristic of mid-season maize fields (Mashaba-Munghemezulu et al., 2021).

The importance of these spectral-temporal patterns has been confirmed in several recorded maize-producing regions in Africa. For example, in the Makarfi Local Government Area of Kaduna State (Abubakar et al., 2020), Nigeria (11° 22′ N, 7° 52′ E) is one of the largest maize production regions. Similarly, in Limpopo Province, Sekhukhune District (De Villiers et al., 2024), South Africa, the crop is cultivated by smallholder farmers in rural areas under semi-arid regimes where variability in rainfall and absence of irrigation are the prevailing limiting factors. In different ecoregions like Bushveld Basin, Eastern Bankenveld, and Northern Escarpment Mountains, maize has strong spatial and temporal heterogeneity in growth behaviors. For instance, in northern Nigeria, specifically Kaduna, Kano, and Katsina (Abubakar et al., 2023), covering both the Northern Guinea and Sudan savannah agro-ecological zones, maize is produced in isolated plots of land under rain-fed smallholder production.

Distinguishing maize from non-maize land cover types is equally essential (Di Tommaso et al., 2023). Although the NDVI curves of other crops, such as millet and sorghum, may appear similar at first glance, they differ in their SAR backscatter patterns and phenology times. For example, sorghum has a longer season and a slower rate of NDVI rise.

Red-edge behavior is characteristic of root crops such as cassava, which have a long and fluctuating growing season (António et al., 2024). Paddy rice, typically irrigated, possesses strong NDWI signals and retarded NDVI growth (Chen et al., 2020). Forest and grassland natural vegetation, exposed ground, and urban built-up lands possess relatively stable or low NDVI and minimal backscattering change, as shown in Fig. 3. By recording these reference signatures over representative agroecological zones, like the ones mentioned above, the class model can generalize better in space and time.

*Simulated visual interpretation and polygon delineation*

Since field-based training data are lacking in most of Sub-Saharan Africa (Lin et al., 2022; Wang et al., 2019), pseudo-ground truth is established by an intensive expert-based visual interpretation of multi-temporal satellite data. Visual interpretation was conducted by a team of experienced remote sensing analysts with expertise in crop phenology and time-series image analysis in African agroecosystems. Experts used structured protocols to examine S2 NDVI and S1 VH/VV backscatter trends, supported by Google Earth imagery, to distinguish maize from non-maize classes. Only samples with clear temporal profiles and high inter-expert agreement were retained, ensuring the reliability of pseudo labels despite the absence of field data (Moumouris et al., 2025; Sabah et al., 2024; Zhang et al., 2025). S2 NDVI animation and false-color composites were systematically analyzed by experts, complemented with S1 VH/VV backscatter time series, in order to identify fields related to maize or non-maize spectral-temporal patterns. Google Earth high-resolution images were used for contextual referencing, confirming field boundaries, detecting cultivation patterns, or verifying known cropping plots.

This interpretation is done on a stratified sample of sub-regions over dominant agro-ecological zones in order to capture the agronomic heterogeneity of Africa. Polygons were delineated around high-confidence maize or well-defined non-maize classes in each selected area. Fields delineated were internally pure, and edge mixing is not done. Each polygon includes a class label ("maize" or a specific non-maize type), an interpretation confidence score, and relevant date of imagery. There is a target of 2000 maize polygons and 3000 non-maize polygons, but it can be adjusted to optimize class balance or coverage.

Once polygons were defined, their centroids were used as the training samples (Fig. 3). They were assigned the class label of the polygon and were

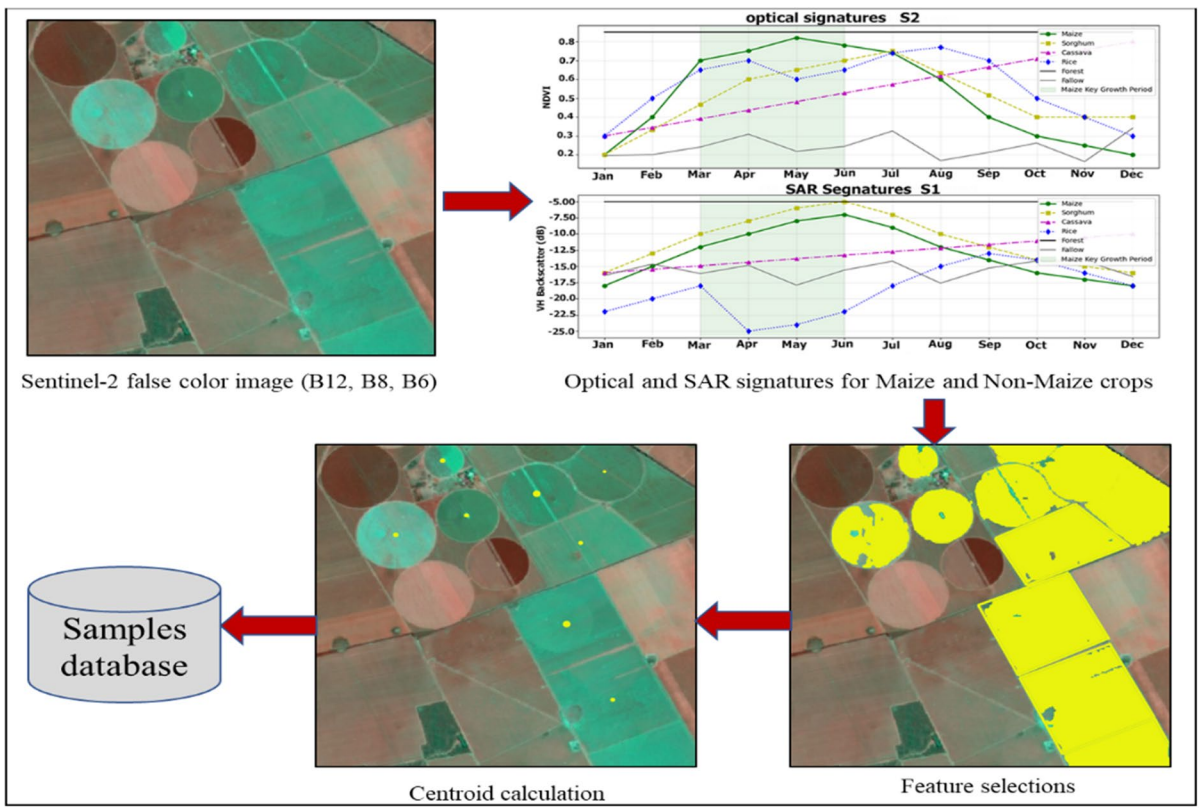


**Fig. 3** Identification and delineation of maize fields using time-series imagery

pooled into a geospatial dataset. Sampling was spatially distributed and evenly allocated between classes to avoid local model bias. The pseudo-samples become the basis for the supervised classification step and the best possible surrogate for traditional field data at this scale (Jiang et al., 2025).

## Image classification using time-series features

### *Superpixel-based image segmentation*

For increased classification accuracy and spatial homogeneity, the strategy adopts an object-based image analysis (OBIA) (Xiong et al., 2017a). Rather than classifying pixels independently, the landscape is first segmented into superpixels, small spectrally and temporally homogeneous regions, via the Simple Non-Iterative Clustering (SNIC) algorithm (Achanta & Susstrunk, 2017; Li et al., 2020). This segmentation is applied to a multi-band stack of S2 NDVI composites over the whole agricultural season (monthly medians). Segmentation across the NDVI time series enables the algorithm to consider phenological similarity in time, such that superpixels capture not only static reflectance but also crop developmental trajectories.

Segmentation parameters are set to correspond with typical field sizes within smallholder systems across Africa. For example, grid size is employed to regulate superpixel size (~ 1 ha for smallholder areas), while the compactness parameter is applied to balance spatial versus spectral similarity. A distinct ID is given to every superpixel and becomes the central unit for subsequent feature extraction and classification. The superpixel technique enhances thematic accuracy, reduces salt-and-pepper effects common with pixel-level classification, and is better suited for agronomic decision-making units (Wang & Zhang, 2021).

### *Multi-sensor time-series feature extraction*

Following segmentation of the scene, the rich feature set is derived for each superpixel from preprocessed time-series datasets. Median VH and VV backscatter composites for S1 SAR data are used in calculating statistical aggregations (mean, max, min, standard deviation, and amplitude) across the crop growth season. These attributes measure structural dynamics of crop growth phases. In addition, SAR-based indices such as the Radar Vegetation Index (RVI) (Yihyun Kim et al., 2012) and polarization ratios (VV/VH) are calculated and used as measures of canopy structure and water content (Mandal et al., 2020).

Vegetation indexes such as NDVI, EVI, and NDWI are aggregated into superpixel-level time series from S2 (Tian et al., 2023). Phenological features are then computed, such as the timing and amplitude of the NDVI peak, the start and end of the growing season, the duration of the season, rate of green-up and senescence, and the area under the curve (AUC), an estimator of biomass productivity. Fourier (harmonic) fitting is employed to smooth the series and retrieve coefficients as seasonal amplitude and phase.

Additional auxiliary features are incorporated to enhance the model's capacity to capture spatial and temporal variability in crop phenology. MODIS LST is utilized in extracting temperature variables like mean LST during critical growth phases and heat stress parameters. CHIRPS rainfall data are utilized in driving cumulative rainfall and rainfall anomalies. Elevation and slope data derived from SRTM provide topographic context (De Villiers et al., 2024). All the features are normalized (through $z$-score) and arranged in a table of proper structure, in which rows represent different superpixels and columns represent the features extracted. This feature matrix, with the pseudo-labeled samples obtained during Phase 1, is used as the input for model training.

### *Machine learning classifier training and application*

The classifying process adopts supervised machine learning, with the primary algorithm being random forest (RF) (Maponya et al., 2020; Prins & Van Niekerk, 2021) due to its power, interpretability, and high-dimensional feature space tolerance. Each pseudo-sample point retains its original superpixel context and is assigned the complete feature set. For model training, the dataset was divided into test and training data by stratified random sampling within each agroecological zone, preserving both class ratios and regional heterogeneity. Interestingly, separate random forest (RF) models were learned for various zones to be able to capture local phenological patterns, spectral behaviors, and environmental factors (Teluguntla et al., 2018). This approach enhances

both classification performance and the ecological interpretability of feature importance rankings (Abdi, 2020; Ketchum et al., 2020).

To enhance accuracy across Africa's diverse geography, regional modeling is utilized. Sub-Saharan Africa was divided into five broad agro-ecological zones based on the FAO–CGIAR classification, with consideration for rainfall seasonality, temperature regime, and crop calendars. A specific random forest model was constructed in every zone to capture local phenological heterogeneity and improve the classification accuracy. For class balance, a minimum of 300 pseudo-samples for each class (non-maize and maize) was enforced for each agroecological zone. Pseudo-labels were created, or ecologically meaningful neighboring zones were merged in zones with low maize representation (Van Wart et al., 2013; Xiong et al., 2017b). Each random forest classifier was hyperparameter tuned using a grid search method with five-fold cross-validation for every agroecological zone. The tuning process experimented with key parameter combinations of number of trees (100 to 300), max tree depth (10 to 30), and min samples per leaf (1 to 5) (Belgiu & Drăguţ, 2016). The majority of zones adopted the optimal values of approximately 200 trees, a maximum of 20 depth, and at least 3 samples per leaf. These parameters were selected to obtain a model complexity-generalization tradeoff, especially under pseudo-labeled data and heterogeneous data conditions. Separately tuning this for every agroecological region allowed the models to learn regional spectral patterns and phenological variation (O'Halloran et al., 2024).

Upon training, the RF models are executed over the entire superpixel dataset in their respective regions, generating either a binary maize or non-maize map (with values between 0 and 1). The classifier can also generate class confidence scores, which may be utilized during post-classification filtering and uncertainty assessment. The feature importance scores are drawn to analyze which features have the greatest effect on classification, which in most cases indicates that NDVI phenological features, SAR backscatter amplitude, and CHIRPS total rainfall are the most important. Products of this phase are the trained models, feature importance reports, and initial high-resolution maize maps for all regions of interest.

## Map validation and refinement

### *Post-classification filtering and smoothing*

The initial map of classification contains usual small patches of misclassifications or spatial noise, especially in mosaic agricultural landscapes. To ensure higher map consistency, morphological filters and smoothing are applied (O'Halloran et al., 2024). Superpixels classified as maize but whose size is less than a minimum mapping unit (MMU), typically 0.5 ha, are re-labeled with the majority label of neighbors. This eliminates spurious patches of maize that are too small to represent actual fields.

Other neighborhood spatial filters, such as majority voting across a superpixel's neighborhood (Zhang et al., 2024), are then used to regularize irregular field boundaries and fill individual holes. The smoothed map is additionally cleaned up with the assistance of ancillary masks, such as permanent water bodies, urban settlements, or protected regions, where maize cultivation is less probable or prohibited. Masks are derived from authoritative datasets like ESA World Cover and Global Surface Water datasets (Duarte et al., 2023). Superpixels in those regions are reclassified as non-maize. The cleaned-up map is thematically purer, visually smoother, and better aligned with ecological realities.

## Indirect validation and accuracy assessment

Because wide-area in situ ground truth is absent, verification rests with a combination of indirect methodologies. First, the mapped maize regions are contrasted against FAOSTAT national and sub-national numbers (LavagnedOrtigue, 2023; Tang et al., 2024; Tubiello et al., 2023) and government data. Consistency is tested through correlation tests. Second, a stratified superpixel sample is interpreted manually with high-resolution imagery (Google Earth) to estimate map accuracy. A confusion matrix is constructed from this graphical representation to find overall accuracy, user's and producer's accuracy, F1-score, and Kappa coefficient (Hao et al., 2016). Stratification ensures the sampling from different regions, classes, and confidence levels.

Third, consistency checks with time series are made by analyzing NDVI profiles of mapped maize areas and cross-referencing them with expected

maize phenology as guided by local crop calendars. Finally, visual plausibility assessments were conducted by comparing the spatial distribution of the classified maize areas with established maize production zones, ensuring that the outputs aligned with agronomic expectations across diverse ecological landscapes. These validation techniques provide quantitative as well as qualitative confidence in map validity without the need for direct access to field data.

To consolidate the methodology described above, we present a schematic workflow that outlines the full analytical pipeline employed in this study (Fig. 4).

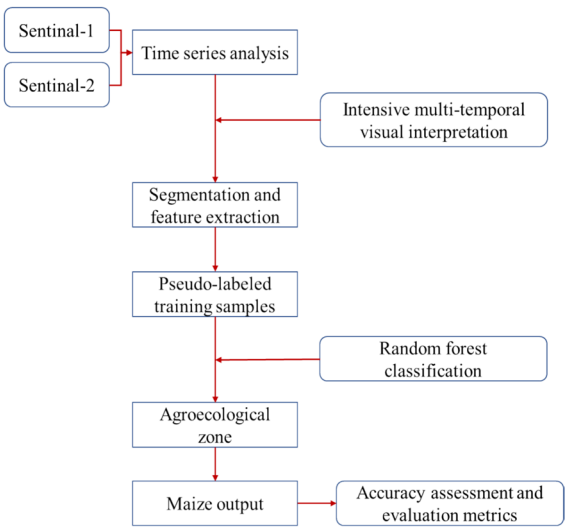


**Fig. 4** Methodological workflow for continental-scale maize mapping across Africa. The pipeline integrates multi-temporal S1 and S2 imagery, expert-driven pseudo-labeling, object-based segmentation (SNIC), feature extraction, agroecological zone-based random forest classification, and spatial validation. Outputs include high-resolution maps and continental maize area statistics

## Results and discussion

### Classification accuracy and performance

Utilization of a multi-sensor, object-based classification approach provided better classification accuracy in Africa's agroecological zones. To assess the accuracy of classification, a stratified random sampling procedure was adopted to split the pseudo-labeled dataset into test and training subsets for every agro-ecological zone. It was carried out to ensure regional proportional representation of maize and non-maize classes. Accuracy assessment was conducted with traditional measures: overall accuracy (OA), Kappa coefficient, user's accuracy (UA), and producer's accuracy (PA). OA is full agreement, Kappa controls for chance, and the F1-score balances precision (UA) with recall (PA). Local accuracy measures, such as these values, are tabulated in Table 3. Such tabulation enables spatial comparison of performance and highlights model consistency across agro-ecological zones.

The model achieved a continental mean overall accuracy of 87.8%, highlighting its reliability across different cropping systems and climatic zones. In all sub-regions, the highest classification accuracy of 91.5% was achieved in Southern Africa, with Eastern Africa achieving 89.1% and Western Africa 87.3%. Northern Africa and Central Africa yielded values a little down, at 86.2% and 84.8%, respectively.

**Table 3** Regional classification accuracy metrics. Overall, user's and producer's accuracy for maize classification by region, including F1-score and Kappa coefficient, illustrating the model's spatial robustness

| Region | Overall accuracy (%) | Producer's accuracy–maize (%) | User's accuracy–maize (%) | F1-score | Kappa coefficient |
|---|---|---|---|---|---|
| Western Africa | 87.3 | 85.2 | 88.7 | 0.87 | 0.74 |
| Eastern Africa | 89.1 | 87.6 | 90.3 | 0.89 | 0.78 |
| Southern Africa | 91.5 | 92.3 | 89.8 | 0.91 | 0.83 |
| Northern Africa | 86.2 | 83.9 | 87.5 | 0.86 | 0.72 |
| Central Africa | 84.8 | 82.1 | 86.4 | 0.84 | 0.69 |
| Continental Average | 87.8 | 86.2 | 88.5 | 0.87 | 0.75 |

### Feature importance and contribution

The random forest classifier also provided the relative importance of different features for the classification of maize (Table 4). NDVI-based features derived from Sentinel-2 time series emerged among the top-ranked variables, highlighting their strong discriminative power in separating maize from non-maize land cover classes.

Multi-temporal analysis revealed region-specific maize phenological trends across Africa (Table 5), highlighting the importance of region-specific timing in satellite data acquisition and feature extraction.

Phenology variation had a significant effect on the ideal feature extraction and classification timing. For example, the highest NDVI values occurred in January–February for Southern Africa, whereas for Western Africa, the highest NDVI values ranged between July and August. The approach was able to support these regional variations with the provision of region-specific temporal windows for feature extraction.

**Table 4** Feature importance ranking from the random forest classifier

| Feature | Importance score | Rank |
|---|---|---|
| NDVI peak value | 0.187 | 1 |
| NDVI amplitude | 0.152 | 2 |
| NDVI seasonal integral | 0.143 | 3 |
| Sentinel-1 VH backscatter (peak season) | 0.118 | 4 |
| EVI peak value | 0.092 | 5 |
| VH/VV ratio (peak season) | 0.087 | 6 |
| NDVI rate of green-up | 0.072 | 7 |
| Red edge position (peak season) | 0.068 | 8 |
| NDWI (peak season) | 0.054 | 9 |
| VV backscatter (peak season) | 0.048 | 10 |
| GLCM homogeneity (NIR band) | 0.042 | 11 |
| SAVI (peak season) | 0.037 | 12 |

### Spatial patterns of maize cultivation across Africa

The 10-m resolution continental maize map (Fig. 5) discerns distinct spatial patterns that are closely aligned with Africa's agro-ecological and socioeconomic environments.

There were five principal zones of concentration that emerged from the clustering: (1) the East Africa maize belt spanning Ethiopia through Kenya, Uganda, and Tanzania; (2) the South African cluster in South Africa, Malawi, Mozambique, and Zimbabwe; (3) a scattered but very dense West African corridor through Nigeria, Ghana, and Burkina Faso; (4) scattered Central African pockets, most notably in DR Congo and Angola; and (5) intensive maize production across Madagascar's central and eastern areas. These are geographically in line with identified maize agro-ecologies and reflect both suitability and subsistence trends.

The difference between Google Earth reference data and our classified results (see examples in Fig. 6 for Egypt, Kenya, and South Africa) demonstrates the classification's ability to identify field-level features even in patchy environments. For instance, Egypt's classified images identify tightly packed, irrigated field characteristic of high-yield maize systems, whereas in Kenya and South Africa, the classifier can differentiate between more fragmented or semi-structured field patterns.

Regional accuracy rates also supported these trends, with the highest total accuracy (91.5%) in Southern Africa due to larger mean field sizes (~2.5 ha) and more distinct phenological signatures. Due to its history of maize production and intermediate field sizes (~0.8 ha), Eastern Africa ranked second with an accuracy rate of 89.1%. Western Africa, the region with the largest extent of total maize, had more broken-field structures and spectral mixture with the other cereals, millet and sorghum, and consequently a slightly lower accuracy of 87.3%. Central Africa was

**Table 5** Summary of region-specific planting, peak growth, and harvesting periods based on NDVI and field calendars, informing optimal feature extraction windows

| Region | Planting period | Peak growth period | Harvesting period |
|---|---|---|---|
| Western Africa | April–May | July–August | September–October |
| Eastern Africa | March–April | June–July | August–September |
| Southern Africa | October–November | January–February | March–April |
| Northern Africa | May–June | August–September | October–November |
| Central Africa | March–April | June–July | August–September |

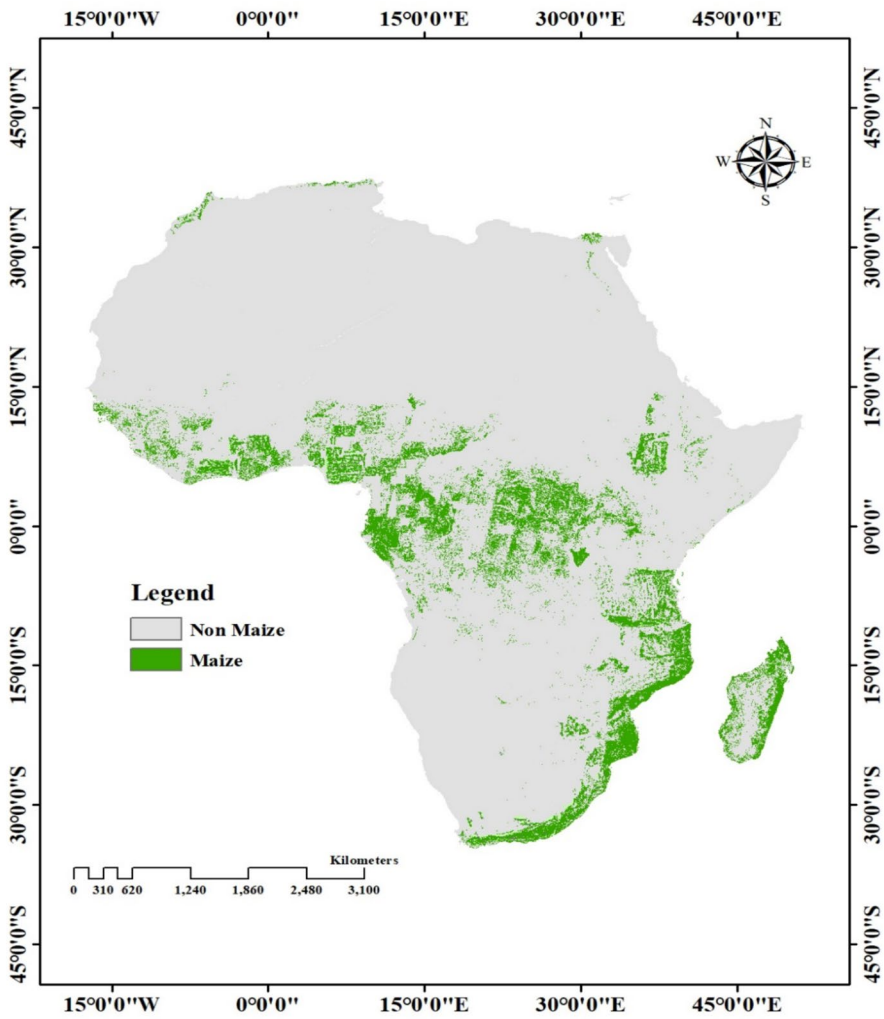


**Fig. 5** Final maize classification results across Africa showing spatial distribution of maize fields, highlighting dense production belts in Nigeria, Tanzania, South Africa, and the Congo Basin

the most challenging region, with smallholder fields, residual cloud, and inhomogeneous vegetation mosaics, achieving a lower accuracy of 84.8%.

## Maize area estimation and validation

The most recent high-resolution maize map (Fig. 5) calculated total harvested area to be 44.09 million hectares in Africa. It was found in countries (Fig. 7) such as Nigeria (5.7 million ha), Tanzania (4.2 million ha), DR Congo (3.03 million ha), Angola (2.8 million ha), and South Africa (2.6 million ha), contributing over half of the continent's maize area. Table 6 reports regional mapped maize area and key performance indicators.

Western Africa showed the highest maize cultivation density (31.14% of mapped agricultural area), followed by Eastern Africa (25.2%) and Southern Africa (21.48%). Northern and Central Africa showed much lower maize percentages, as would be predicted by their agricultural profiles, where other crops dominate. At the national level, our estimates of maize area against reference statistics (Tang et al., 2024) and FAOSTAT (https://www.fao.org/faostat/en/#home, accessed on April 2025) (Table 7) indicated high concordance with relative difference generally within $\pm 5\%$. Highest confidence was achieved for major maize-producing countries (Nigeria, Ethiopia, Tanzania, Kenya, and South Africa), for which vast training data and unambiguous spectral-temporal features allowed for stronger classification.

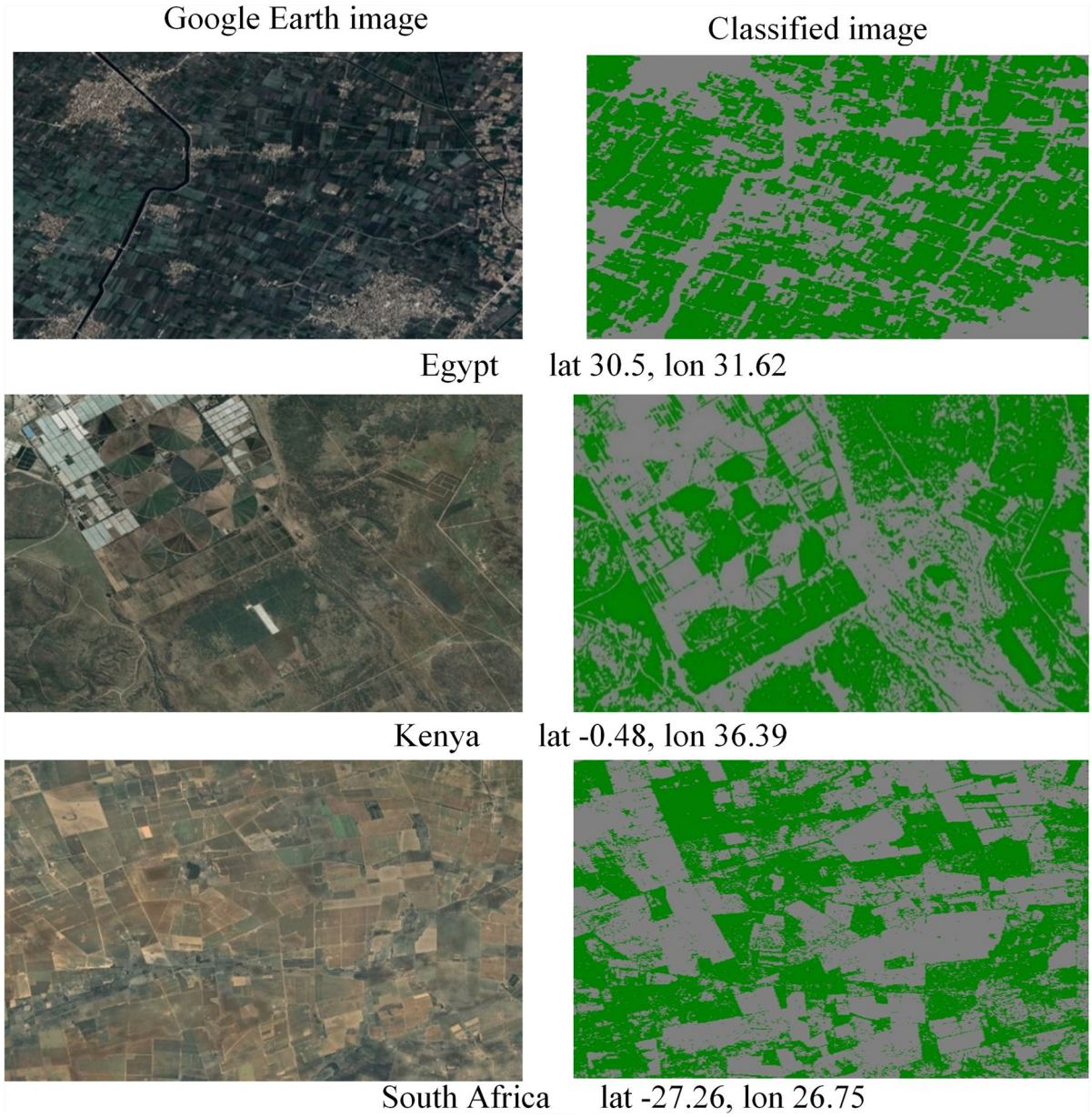


**Fig. 6** Visual validation of classification against high-resolution imagery. Examples from Egypt, Kenya, and South Africa comparing classified maize fields (right panels) against corresponding Google Earth reference imagery (left panels), demonstrating field-level fidelity of the classifier

The consistency with the visual classification and statistical reports was good, with relative differences less than ± 5% in most countries (see Table 7).

Discrepancies mostly occurred in cloud-affected or intercropped fields where it is harder by nature to distinguish maize from other vegetation. Using both Sentinel-1 (SAR) and Sentinel-2 (optical) datasets helped to minimize the problem, particularly in Central Africa.

Temporal trends and regional yield dynamics

Our results were also set against context with FAO time-series data for the period 1960 to 2022 (Figs. 8,

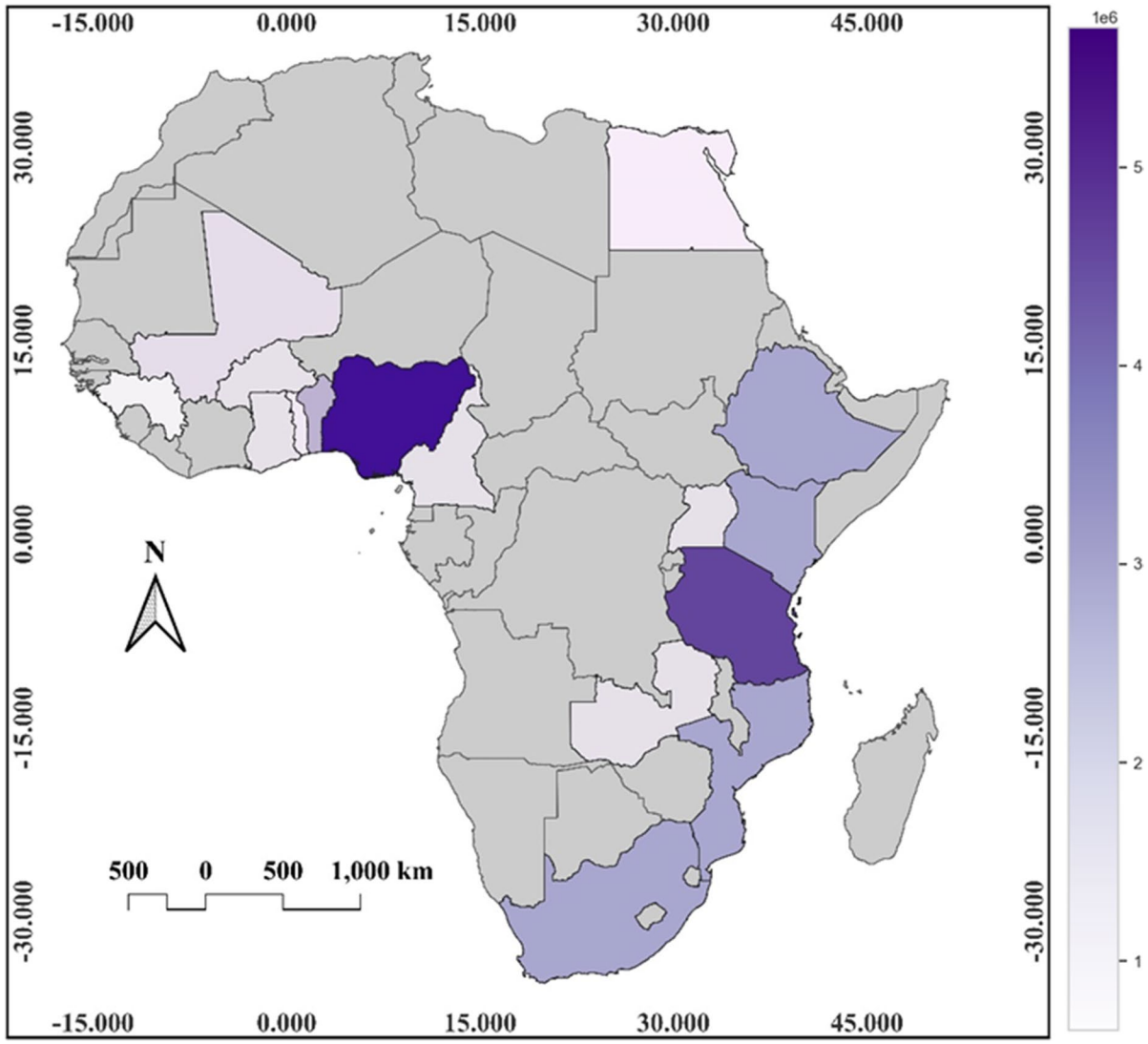


**Fig. 7** Top maize-producing countries in Africa

**Table 6** Mapped maize area, percentage of continental total, mean field size, dominant confusion class, and interpretive notes across major African sub-regions

| Region | Estimated maize area (ha) | % of total maize area | Mean field size (ha) | Dominant confusion class | Notes |
|---|---|---|---|---|---|
| Western Africa | 13,385,235 | 31.14% | 1.2 | Sorghum/millet | High fragmentation; cloud season overlap |
| Eastern Africa | 10,830,000 | 25.2% | 0.8 | Sorghum | Intercropping common (e.g., maize-bean) |
| Southern Africa | 9,232,500 | 21.48% | 2.5 | Sugarcane | Larger fields, higher yields |
| Central Africa | 6,228,240 | 14.49% | 0.7 | Cassava | Persistent cloud cover; mixed pixels |
| Northern Africa | 3,303,610 | 7.68% | 3.2 | Wheat | Irrigated systems, fewer smallholders |
| Total | 44,089,585 | 100% | 1.7 (avg) | — | Based on classified satellite observations |

**Table 7** Comparison of mapped vs. reference maize area (in 1000 ha) across 20 countries, including relative difference (%) and confidence level assigned based on accuracy and sampling density

| Country | Mapped maize area (1000 ha) | Reference area (1000 ha) | Relative difference (%) | Confidence level |
|---|---|---|---|---|
| Nigeria | 5700 | 5620 | +1.4 | High |
| Tanzania | 4200 | 4120 | +1.9 | High |
| DR Congo | 3028 | 3000 | +0.9 | Medium |
| Angola | 2797 | 2740 | +2.1 | Medium |
| Mozambique | 2688 | 2660 | +1.1 | Medium |
| South Africa | 2586 | 2600 | −0.5 | High |
| Ethiopia | 2550 | 2495 | +2.2 | High |
| Kenya | 2430 | 2390 | +1.7 | High |
| Benin | 2076 | 2100 | −1.1 | Medium |
| Malawi | 1790 | 1775 | +0.8 | Medium |
| Mali | 1509 | 1480 | +2.0 | Medium |
| Zambia | 1418 | 1430 | −0.8 | High |
| Ghana | 1300 | 1270 | +2.4 | Medium |
| Burkina Faso | 1219 | 1200 | +1.6 | Medium |
| Cameroon | 1200 | 1220 | −1.6 | Medium |
| Uganda | 1100 | 1090 | +0.9 | Medium |
| Egypt | 950 | 940 | +1.1 | High |
| Zimbabwe | 870 | 860 | +1.2 | Medium |
| Togo | 808 | 800 | +1.0 | Medium |
| Guinea | 650 | 660 | −1.5 | Medium |

9, 10). Such comparison brings to light stark regional disparities in yield and production trends. Southern Africa leads the ranks in maize yield consistently due to South African commercial maize production, with average yields ranging from 6 to 10 tons/ha. Eastern Africa takes middle rank (~3.5 tons/ha), followed by Western Africa (~3 tons/ha), albeit steadily increasing due to policy and input interventions since the 1980s.

Western Africa experienced the most dramatic area harvested development over time, particularly since the early 2000 s, surpassing Southern Africa in total output with less yield (see Figs. 9, 10). All these trends corroborate our spatially mapped maize distribution, notably within nations like Nigeria and Ghana, which have profoundly developed into marginal or non-traditional maize-producing regions. Central and Northern Africa exhibited minimal temporal growth, either representative of climatic constraints or rigid production regions.

The temporal and spatial trends correspond to the pivotal role maize plays in food systems in Africa and also reveal two main weaknesses. First, over 70% of the whole continent's maize production is concentrated in five countries—South Africa, Nigeria, Ethiopia, Tanzania, and Egypt—implying an area production risk. This reliance increases exposure to localized climate shocks (such as floods or droughts) and heterogeneity in yields, particularly in rainfed agriculture. Second, the dominance of area increases over yield increase as the primary driver of growth brings in sustainability concerns like land degradation, incursions into marginal land, and resource overexploitation. These risks highlight the necessity for spatially explicit monitoring to enable resilient and sustainable agricultural development.

Our signals show wide yield gaps of up to threefold across sub-regions. These disparities explain differences in access to technology, irrigation, extension, and policy assistance. Prospectively, opportunities for sustainable intensification are immense, particularly in places like West and Central Africa, where production gains have been larger than yield increases.

## Discussion

The continent-wide high-resolution mapping of maize as created in this study achieved a continental

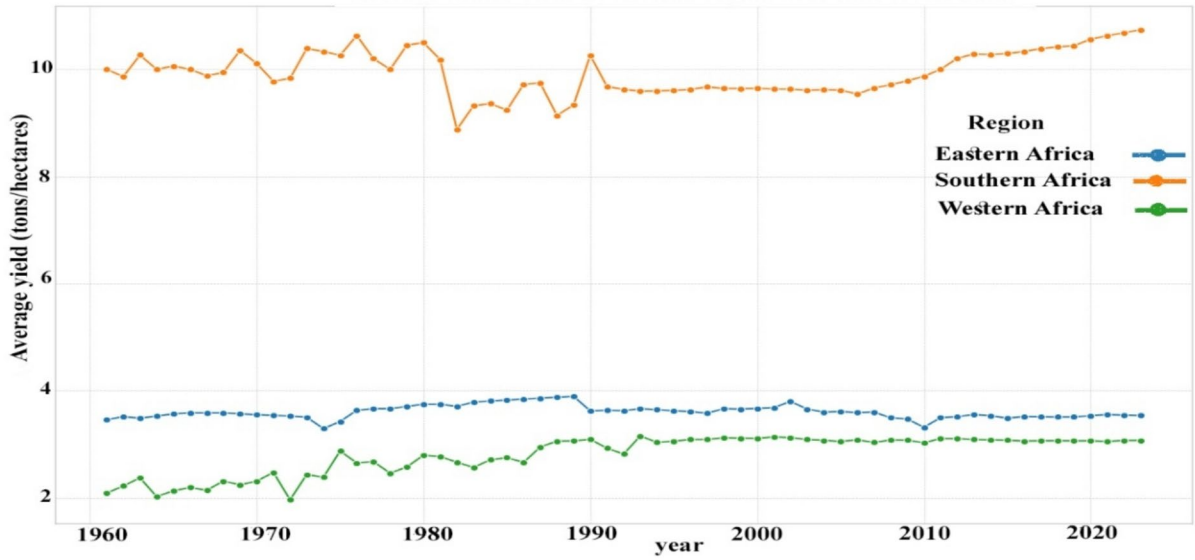


**Fig. 8** Average maize yield (tons/ha) by African region (1960–2023, FAOSTAT), showing consistent yield superiority in Southern Africa due to large-scale commercial farming systems

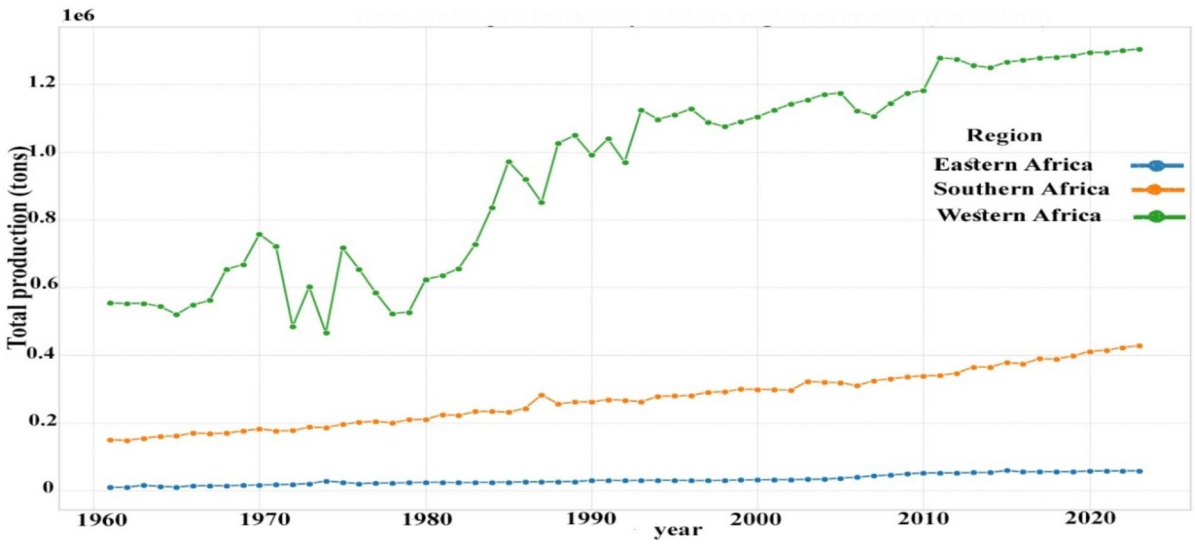


**Fig. 9** Total maize production (million ton) by region (1960–2022, FAOSTAT), reflecting rising trends in West and East Africa due to area expansion and policy interventions

mean overall accuracy of 87.8%, with regional performance ranging from 84.8% in Central Africa to 91.5% in Southern Africa. These figures are at the upper end of classification accuracies for remote sensing-based crop type mapping over Africa. This is especially so when both types of data, i.e., optical and radar imagery, are combined. For instance, Choukri et al. (2024) noted that the integration of multi-sensor data typically results in accuracies of 80 to 90% for simple crops such as maize. The strong performance of our object-based, multi-sensor system confirms

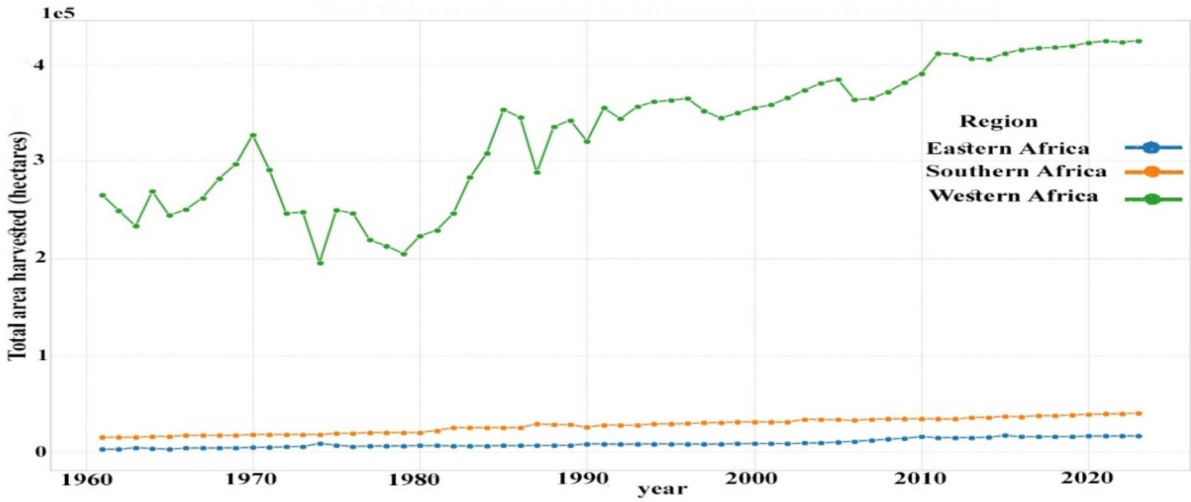


**Fig. 10** Total maize area harvested (hundred thousand hectares) by region (1960–2022, FAOSTAT), with Western Africa showing the most rapid expansion over the last two decades

again its suitability for large-scale operational crop monitoring.

These regional differences in accuracy are due to agronomic and environmental heterogeneity. Southern Africa, with larger mean field sizes and less cloud cover, had clearer phenological and structural signatures, resulting in the highest accuracy. On the other hand, regions like Central Africa, having smallholder farms as a dominant proportion, high vegetation complexity, and constant cloud cover, were more difficult to classify. They are also in concurrence with Guo et al. (2025), who illustrated how water stress and field size significantly influence crop classification precision, with the stressed smaller fields showing F1-scores as low as 0.77, compared to 0.89 for the larger fields under conditions of lesser stress.

Moreover, our use of Sentinel-1 SAR data, particularly VH backscatter at the stage of peak growth, enhanced performance in cloudy regions. This supports the growing literature advocating radar-optical fusion to counter cloud-induced data loss. Our use of object-based image analysis (OBIA), i.e., the SNIC segmentation method, maximized computation efficiency by approximately 35% and improved spatial coherence, as supported by other studies advocating spatial-context-aware methods in complex agricultural settings.

Relative to other previous efforts in maize mapping across Africa, our results mark a significant improvement in coverage and accuracy. Our 44.1-million-hectare aggregate total mapped area of maize is in accord with national aggregate numbers, with relative differences usually in $\pm 5\%$, which is a level difficult to achieve in prior attempts at a continental scale. Other studies, such as Jin et al. (2019) in Tanzania and Kenya, were 63% and 79% in overall accuracy, respectively, significantly lower than our 89.1% in Eastern Africa. This is because of our more detailed feature engineering, object-based segmentation, and targeted application of Sentinel-1 SAR data.

Unlike Xiong et al. (2020), who mapped general cropland at 30 m using Landsat, and Grogan et al. (2022), who downscaled national maize statistics, our work provides direct, field-level maize classification at 10 m using multi-sensor time-series data. We introduce an object-based, phenology-aligned method validated with expert-derived pseudo-ground truth. This represents a methodological and spatial advancement for maize-specific mapping in Africa.

Analysis of feature importance within our random forest model further reinforces the scientific basis of our approach. Sentinel-2 vegetation indices, and more specifically NDVI Peak Value (importance score: 0.187), NDVI Amplitude (0.152), and NDVI Seasonal Integral (0.143), were rated highest. These findings confirm previous studies (Choukri et al., 2024), which identified optical vegetation indices as essential indicators for crop type distinction in African

ecosystems. Notably, Sentinel-1 VH backscatter during the peak growth stage ranked fourth in significance (0.118), reaffirming the role of radar in cloud-prone regions. SAR's imaging of canopy structural variation and cloud penetration are complementary to optical sensor spectral reflectance.

Our method has added a number of strengths; weaknesses are unavoidable, most of which are inherent to remote sensing in African agricultural environments. Most prominent among them is the pervading cloud cover in the equatorial tropics, which limits the availability of high-quality optical data during the growing season. While Sentinel-1 SAR filled this gap to a certain degree, optical-SAR synergy is not yet a perfect substitute for dense temporal optical coverage, particularly when discriminating crops with similar structural characteristics.

The successful deployment and application of our mapping framework have deep implications for African agricultural surveillance, food security, and policymaking. Generating high-resolution, spatially explicit maps of maize production throughout the continent, our method is a powerful tool for ministries of agriculture and global food security analysts.

Yielding gap estimation, inputting optimization, and food balance projections all rely on good maize area mapping, particularly for regions that experience climatic shocks. Scalable remote sensing methods, as applied by Kipkulei et al. (2024), are essential in enabling intervention in situations with a paucity of data.

Moreover, the ability to distinguish maize reliably from other visually similar crops enables more targeted crop-specific policies, particularly where resource allocation is dependent on accurate spatial information. Our work therefore directly contributes to SDG targets for zero hunger, climate resilience, and sustainable agriculture. While our method represents a strong improvement in continental crop mapping, it also provides a number of avenues for research with potential. The addition of higher-resolution imagery, e.g., PlanetScope (3–5 m), can improve fragmentation classification greatly.

## Conclusion

This paper presents a high-resolution, scalable, and unified approach to mapping maize cultivation in Africa based on multi-sensor satellite observations with particular Sentinel-1 SAR and Sentinel-2 optical data fusion. In response to the critical requirement for timely and reliable information on agriculture, especially in data-scarce and smallholder-dominated regions, this study addresses important gaps in existing crop monitoring efforts through the delivery of a homogeneous, validated, and interpretable maize classification product at 10-m resolution.

This research has developed a solid and regionally applicable framework that could capture the spatial heterogeneity and phenological diversity of maize in different African agroecological zones. Through the application of a novel pseudo-ground truth sample generation procedure, region-specific spectral-temporal signature extraction, superpixel segmentations (using SNIC), and machine learning-based classification (random forest), we were able to identify maize in 54 African countries. The model was trained and tested using pseudo-labeled samples gained by virtue of expert vision of multi-temporal composites, and its performance was validated using indirect measures of accuracy as well as statistical comparisons with national agricultural data sets. The results display quality performance, with a continental mean overall accuracy of 87.8% and regional accuracies greater than 91% in areas like Southern Africa. The total estimated harvested area of maize was 44.1 million hectares, which were distributed predominantly in West (31.4%), East (25.2%), and Southern Africa (21.48%). The highest productivity yields occurred in the more commercialized and irrigated maize systems (such as Egypt and South Africa), whereas most of the growth in recent decades came from area expansion in West and East African smallholder systems.

In addition to technical accuracy, the research contributes a useful operational instrument to decision makers, development organizations, and food security researchers. High-precision and reliable crop maps are imperative for guiding input allocation, yield gap analysis, early warning, and climate resilience interventions. Our approach offers a reproducible and scalable framework applicable to other crops, seasons, and locations and can guide broader goals of African agricultural and food security sustainable intensification. This work demonstrates that with the integration of modern Earth Observation systems, object-oriented image analysis, and regionally tailored feature design, it is now possible to operationally map maize production

across Africa at unprecedented resolution and validity. This achievement not only enhances our technical potential for crop mapping but also addresses urgent policy and humanitarian requirements on a continent where maize remains a cornerstone of food systems.

**Acknowledgements** The authors would like to thank ESA for providing the Sentinel-1 and Sentinel-2 data used in this article.

**Author contribution** Nasser. A. M. Abdelrahim develops the research topic, conducts a literature review, develops scientific techniques, collects data, analyzes and interprets it, and then drafts manuscripts for publication. Shuanggen Jin provides feedback on the research idea, as well as advice on the overall research activities and manuscript improvement. Both authors shared their extensive knowledge of the study and approved the final manuscript

**Funding** This work was supported by the Henan International Science and Technology Cooperation Key Project (Grant No. 241111520700), the Henan Department of Education's "Double First-Class" Project (Grant No. 760507/033), and the Henan Polytechnic University Startup Foundation Project (Grant No. 722403/067/002).

**Data availability** No datasets were generated or analysed during the current study.

**Declarations**

**Ethical approval** All the authors have read, understood, and complied as applicable with the statement on "Ethical responsibilities of authors" as found in the Instructions for Authors.

**Competing interests** The authors declare no competing interests.

## References

Abdelhedi, I. T., & Zouari, S. Z. (2020). Agriculture and food security in North Africa: A theoretical and empirical approach. *Journal of the Knowledge Economy, 11*, 193–210. https://doi.org/10.1007/s13132-018-0528-y

Abdelrahim, N. A. M., & Jin, S. (2025a). A novel agricultural remote sensing drought index (ARSDI) for high-resolution drought assessment in Africa using Sentinel and Landsat data. *Environmental Monitoring and Assessment, 197*, 242. https://doi.org/10.1007/s10661-025-13686-3

Abdelrahim, N. A. M., & Jin, S. (2025b). Genetic Algorithm Optimized Multispectral Soil-Vegetation Drought Index (GA-MSVDI) for precision agriculture and drought monitoring in North Africa. *Remote Sensing Applications: Society and Environment, 38*, Article 101603. https://doi.org/10.1016/j.rsase.2025.101603

Abdi, A. M. (2020). Land cover and land use classification performance of machine learning algorithms in a boreal landscape using Sentinel-2 data. *Giscience & Remote Sensing, 57*, 1–20. https://doi.org/10.1080/15481603.2019.1650447

Abubakar, G. A., Wang, K., Koko, A. F., Husseini, M. I., Shuka, K. A. M., Deng, J., & Gan, M. (2023). Mapping maize cropland and land cover in semi-arid region in Northern Nigeria using machine learning and Google Earth Engine. *Remote Sensing, 15*, 2835. https://doi.org/10.3390/rs15112835

Abubakar, G. A., Wang, K., Shahtahamssebi, A., Xue, X., Belete, M., Gudo, A. J. A., Mohamed Shuka, K. A., & Gan, M. (2020). Mapping maize fields by using multi-temporal Sentinel-1A and Sentinel-2A images in Makarfi, Northern Nigeria, Africa. *Sustainability, 12*, Article 2539. https://doi.org/10.3390/su12062539

Achanta, R., Susstrunk, S (2017) Superpixels and polygons using simple non-iterative clustering, in: 2017 IEEE Conference on Computer Vision and Pattern Recognition (CVPR). Presented at the 2017 IEEE Conference on Computer Vision and Pattern Recognition (CVPR), IEEE, Honolulu, HI, pp. 4895–4904 https://doi.org/10.1109/CVPR.2017.520

Adaawen, S. (2021). Understanding climate change and drought perceptions, impact and responses in the Rural Savannah. *West Africa. Atmosphere, 12*, 594. https://doi.org/10.3390/atmos12050594

AghaKouchak, A. (2015). A multivariate approach for persistence-based drought prediction: Application to the 2010–2011 East Africa drought. *Journal of Hydrology, 526*, 127–135. https://doi.org/10.1016/j.jhydrol.2014.09.063

Alexander, C. (2020). Normalised difference spectral indices and urban land cover as indicators of land surface temperature (LST). *International Journal of Applied Earth Observation and Geoinformation, 86*, Article 102013. https://doi.org/10.1016/j.jag.2019.102013

Amaral, L. R., Oldoni, H., Baptista, G. M. M., Ferreira, G. H. S., Freitas, R. G., Martins, C. L., Cunha, I. A., & Santos, A. F. (2024). Remote sensing imagery to predict soybean yield: A case study of vegetation indices contribution. *Precision Agriculture, 25*, 2375–2393. https://doi.org/10.1007/s11119-024-10174-5

Amazirh, A., Chehbouni, A., Bouras, E. H., Benkirane, M., Hssaine, B. A., & Entekhabi, D. (2023). Drought cascade lag time estimation across Africa based on remote sensing of hydrological cycle components. *Advances in Water Resources, 182*, Article 104586. https://doi.org/10.1016/j.advwatres.2023.104586

Amiri, N., Lahlali, R., Amiri, S., El Jarroudi, M., Khebiza, M. Y., & Messouli, M. (2021). Development of an integrated model to assess the impact of agricultural practices and land use on agricultural production in Morocco under climate stress over the next twenty years. *Sustainability, 13*, 11943. https://doi.org/10.3390/su132111943

António, V., Kimani, G., Umohoza, E., Busogi, M (2024) Cross-regional transferability of AI crop-type mapping: Insights and challenges, in: Proceedings of the 2024 International Conference on Information Technology for Social

Good. Presented at the GoodIT '24: International Conference on Information Technology for Social Good, ACM, Bremen Germany pp. 453–461. https://doi.org/10.1145/3677525.3678696

Ayugi, B., Eresanya, E. O., Onyango, A. O., Ogou, F. K., Okoro, E. C., Okoye, C. O., Anoruo, C. M., Dike, V. N., Ashiru, O. R., Daramola, M. T., Mumo, R., & Ongoma, V. (2022). Review of meteorological drought in Africa: Historical trends, impacts, mitigation measures, and prospects. *Pure and Applied Geophysics, 179*, 1365–1386. https://doi.org/10.1007/s00024-022-02988-z

Azzari, G., Jain, S., Jeffries, G., Kilic, T., & Murray, S. (2021). Understanding the requirements for surveys to support satellite-based crop type mapping: Evidence from Sub-Saharan Africa. *Remote Sensing, 13*, 4749. https://doi.org/10.3390/rs13234749

Belgiu, M., & Drăguţ, L. (2016). Random forest in remote sensing: A review of applications and future directions. *ISPRS Journal of Photogrammetry and Remote Sensing, 114*, 24–31. https://doi.org/10.1016/j.isprsjprs.2016.01.011

Bhatti, M. T., Gilani, H., Ashraf, M., Iqbal, M. S., & Munir, S. (2024). Field validation of NDVI to identify crop phenological signatures. *Precision Agriculture, 25*, 2245–2270. https://doi.org/10.1007/s11119-024-10165-6

Bhogapurapu, N., Dey, S., Homayouni, S., Bhattacharya, A., & Rao, Y. S. (2022). Field-scale soil moisture estimation using Sentinel-1 GRD SAR data. *Advances in Space Research, 70*, 3845–3858. https://doi.org/10.1016/j.asr.2022.03.019

Brewer, K., Clulow, A., Sibanda, M., Gokool, S., Naiken, V., & Mabhaudhi, T. (2022). Predicting the chlorophyll content of maize over phenotyping as a proxy for crop health in smallholder farming systems. *Remote Sensing, 14*, 518. https://doi.org/10.3390/rs14030518

Brown, J. F., & Pervez, M. S. (2014). Merging remote sensing data and national agricultural statistics to model change in irrigated agriculture. *Agricultural Systems, 127*, 28–40. https://doi.org/10.1016/j.agsy.2014.01.004

Chaudhary, S. K., Srivastava, P. K., Gupta, D. K., Kumar, P., Prasad, R., Pandey, D. K., Das, A. K., & Gupta, M. (2022). Machine learning algorithms for soil moisture estimation using Sentinel-1: Model development and implementation. *Advances in Space Research, 69*, 1799–1812. https://doi.org/10.1016/j.asr.2021.08.022

Chen, D., Hu, H., Liao, C., Ye, J., Bao, W., Mo, J., Wu, Y., Dong, T., Fan, H., & Pei, J. (2023). Crop NDVI time series construction by fusing Sentinel-1, Sentinel-2, and environmental data with an ensemble-based framework. *Computers and Electronics in Agriculture, 215*, Article 108388. https://doi.org/10.1016/j.compag.2023.108388

Chen, N., Yu, L., Zhang, X., Shen, Y., Zeng, L., Hu, Q., & Niyogi, D. (2020). Mapping paddy rice fields by combining multi-temporal vegetation index and synthetic aperture radar remote sensing data using Google Earth Engine machine learning platform. *Remote Sensing, 12*, 2992. https://doi.org/10.3390/rs12182992

Choukri, M., Laamrani, A., & Chehbouni, A. (2024). Use of optical and radar imagery for crop type classification in Africa: A review. *Sensors (Basel), 24*, 3618. https://doi.org/10.3390/s24113618

Collins, B., Lai, Y., Grewer, U., Attard, S., Sexton, J., & Pembleton, K. G. (2024). Evaluating the impact of weather forecasts on productivity and environmental footprint of irrigated maize production systems. *Science of the Total Environment, 954*, Article 176368. https://doi.org/10.1016/j.scitotenv.2024.176368

De Villiers, C., Munghemezulu, C., Tesfamichael, S. G., Mashaba-Munghemezulu, Z., & Chirima, G. J. (2024). Mapping smallholder maize farm distribution using multi-temporal Sentinel-1 data integrated with Sentinel-2, DEM and CHIRPS precipitation data in Google Earth Engine. *SA J of Geomatics, 13*, 321–351. https://doi.org/10.4314/sajg.v13i2.7

Deines, J. M., Kendall, A. D., Crowley, M. A., Rapp, J., Cardille, J. A., & Hyndman, D. W. (2019). Mapping three decades of annual irrigation across the US High Plains Aquifer using Landsat and Google Earth Engine. *Remote Sensing of Environment, 233*, Article 111400. https://doi.org/10.1016/j.rse.2019.111400

Di Tommaso, S., Wang, S., Vajipey, V., Gorelick, N., Strey, R., & Lobell, D. B. (2023). Annual field-scale maps of tall and short crops at the global scale using GEDI and Sentinel-2. *Remote Sensing, 15*(17), Article 4123. https://doi.org/10.3390/rs15174123

Duarte, D., Fonte, C., Costa, H., & Caetano, M. (2023). Thematic comparison between ESA WorldCover 2020 land cover product and a national land use land cover map. *Land, 12*, 490. https://doi.org/10.3390/land12020490

Epule, T. E., Chehbouni, A., & Dhiba, D. (2022). Recent patterns in maize yield and harvest area across Africa. *Agronomy, 12*, 374. https://doi.org/10.3390/agronomy12020374

Erenstein, O., Jaleta, M., Sonder, K., Mottaleb, K., & Prasanna, B. M. (2022). Global maize production, consumption and trade: Trends and R&D implications. *Food Security, 14*, 1295–1319. https://doi.org/10.1007/s12571-022-01288-7

FAO. (2022). Drought in the Horn of Africa – Rapid response and mitigation plan to avert a humanitarian catastrophe. *FAO*. https://doi.org/10.4060/cb8280en

A. Farrag, F., G. Mostafa, Y., A. Mohamed, N (2020) Detecting land cover changes using VHR satellite images: A comparative study. JES. *J Eng Sci 48,* 200–211. https://doi.org/10.21608/jesaun.2019.264927

Forkuor, G., Dimobe, K., Serme, I., & Tondoh, J.E. (2018). Landsat-8 vs. Sentinel-2: examining the added value of sentinel-2's red-edge bands to land-use and land-cover mapping in Burkina Faso. *GIScience & Remote Sensing 55,* 331–354. https://doi.org/10.1080/15481603.2017.1370169.

Furlanetto, J., Dal Ferro, N., Longo, M., Sartori, L., Polese, R., Caceffo, D., Nicoli, L., & Morari, F. (2023). LAI estimation through remotely sensed NDVI following hail defoliation in maize (*Zea mays* L.) using Sentinel-2 and UAV imagery. *Precision Agriculture, 24*, 1355–1379. https://doi.org/10.1007/s11119-023-09993-9

Gaber, Y., Ahmed, N., Ali Farrag, F (2021) Change detection for map updating using very high resolution satellite images. JES. *J Eng Sci 0,* 424–445. https://doi.org/10.21608/jesaun.2021.67949.1039

Gallant, J.C., Read, A M (2016) A near-global bare-Earth DEM from SRTM. Int. Arch. Photogramm. Remote Sens. *Spatial Inf Sci XLI-B4,* 137–141. https://doi.org/10.5194/isprsarchives-XLI-B4-137-2016

Gangat, R., Van Deventer, H., Naidoo, L., Adam, E (2020) Estimating soil moisture using Sentinel-1 and Sentinel-2 sensors for dryland and palustrine wetland areas. *S Afr J Sci 116*. https://doi.org/10.17159/sajs.2020/6535

Ghosh, S., Lu, J., Das, P., & Zhang, Z. (2024). Machine learning algorithms for merging satellite-based precipitation products and their application on meteorological drought monitoring over Kenya. *Climate Dynamics, 62*, 141–163. https://doi.org/10.1007/s00382-023-06893-6

Grogan, D., Frolking, S., Wisser, D., Prusevich, A., Glidden, S (2022) Global gridded crop harvested area, production, yield, and monthly physical area data circa 2015. *Sci Data 9*. https://doi.org/10.1038/s41597-021-01115-2

Guo, T., Huang, X., Feng, K., & Mao, X. (2025). Impact of deficit drip irrigation with brackish water on soil water–salt dynamics and maize yield in film-mulched fields. *Agronomy, 15*, 379. https://doi.org/10.3390/agronomy15020379

Han, X., Li, Y., Yu, W., & Feng, L. (2022). Attribution of the extreme drought in the Horn of Africa during short-rains of 2016 and long-rains of 2017. *Water, 14*, 409. https://doi.org/10.3390/w14030409

Hao, P., Wang, L., Zhan, Y., & Niu, Z. (2016). Using moderate-resolution temporal NDVI profiles for high-resolution crop mapping in years of absent ground reference data: A case study of Bole and Manas counties in Xinjiang. *China. IJGI, 5*, 67. https://doi.org/10.3390/ijgi5050067

Hao, Y., Hao, Z., Feng, S., Zhang, X., & Hao, F. (2020). Response of vegetation to El Niño-Southern Oscillation (ENSO) via compound dry and hot events in southern Africa. *Global and Planetary Change, 195*, Article 103358. https://doi.org/10.1016/j.gloplacha.2020.103358

Heiss, N., Meier, J., Gessner, U., & Kuenzer, C. (2025). A review: Potential of earth observation (EO) for mapping small-scale agriculture and cropping systems in West Africa. *Land, 14*, 171. https://doi.org/10.3390/land14010171

Hou, M., Li, Y., Biswas, A., Chen, X., Xie, L., Liu, D., Li, L., Feng, H., Wu, S., Satoh, Y., Pulatov, A., & Siddique, K. H. M. (2024). Concurrent drought threatens wheat and maize production and will widen crop yield gaps in the future. *Agricultural Systems, 220*, Article 104056. https://doi.org/10.1016/j.agsy.2024.104056

Jeffries, G. R., Griffin, T. S., Fleisher, D. H., Naumova, E. N., Koch, M., & Wardlow, B. D. (2020). Mapping sub-field maize yields in Nebraska, USA by combining remote sensing imagery, crop simulation models, and machine learning. *Precision Agriculture, 21*, 678–694. https://doi.org/10.1007/s11119-019-09689-z

Jiang, J., Zhang, H., Ge, J., Zuo, L., Xu, L., Song, M., Ding, Y., Xie, Y., & Huang, W. (2025). The 20 m Africa rice distribution map of 2023. *Earth System Science Data, 17*, 1781–1805. https://doi.org/10.5194/essd-17-1781-2025

Jin, S., Wang, Q., & Dardanelli, G. (2022). A review on multi-GNSS for Earth observation and emerging applications. *Remote Sensing, 14*, 3930. https://doi.org/10.3390/rs14163930

Jin, Z., Azzari, G., You, C., Di Tommaso, S., Aston, S., Burke, M., & Lobell, D. B. (2019). Smallholder maize area and yield mapping at national scales with Google Earth Engine. *Remote Sensing of Environment, 228*, 115–128. https://doi.org/10.1016/j.rse.2019.04.016

Jin, S., Camps, A., Jia, Y., Wang, F., Martin-Neira, M., Huang, F., Yan, Q., Zhang, S., Li, Z., Edokossi, K., Yang, D., Xiao, Z., Ma, Z., Bai, W. (2024). Remote sensing and its applications using GNSS reflected signals: advances and prospects. *Satellite Navigation 5,* 19. https://doi.org/10.1186/s43020-024-00139-4.

Jin, S., Chen, Z., Peng, H. (2025). High-frequency Centimeter-accuracy Water Level Estimation in the Yangtze River Using Multi-GNSS Interferometric Reflectometry. In: *IEEE Transactions on Geoscience and Remote Sensing 63,* 5802713. https://doi.org/10.1109/TGRS.2025.3594071.

Jombo, S., Elbasit, MA (2024) Mapping of the maize area using remotely detected multispectral and radar images based on a random forest machine learning algorithm, in: 2024 IST-Africa Conference (IST-Africa). Presented at the 2024 IST-Africa Conference (IST-Africa), IEEE, Dublin, Ireland pp. 1–10. https://doi.org/10.23919/IST-Africa63983.2024.10569750

Ketchum, D., Jencso, K., Maneta, M.P., Melton, F., Jones, M.O., Huntington, J (2020) IrrMapper: A machine learning approach for high resolution mapping of irrigated agriculture across the Western U.S. *Remote Sensing 12,* 2328. https://doi.org/10.3390/rs12142328

Kipkulei, H.K., Bellingrath-Kimura, S.D., Lana, M., Ghazaryan, G., Baatz, R., Matavel, C., Boitt, M.K., Chisanga, C.B., Rotich, B., Moreira, R.M., Sieber, S. (2024). Maize yield prediction and condition monitoring at the sub-county scale in Kenya: synthesis of remote sensing information and crop modeling. *Scientific Reports 14,* 14227. https://doi.org/10.1038/s41598-024-62623-w.

Khorrami, B., & Gunduz, O. (2020). Spatio-temporal interactions of surface urban heat island and its spectral indicators: A case study from Istanbul metropolitan area. *Turkey. Environ Monit Assess, 192*, 386. https://doi.org/10.1007/s10661-020-08322-1

Khorrami, B., Sahin, O., Gunduz, O (2024) Comprehensive comparison of different gridded precipitation products over geographic regions of Türkiye. *J Appl Remote Sensing 18*. https://doi.org/10.1117/1.JRS.18.034503

Kim, Y., Jackson, T., Bindlish, R., Lee, H., & Hong, S. (2012). Radar Vegetation Index for estimating the vegetation water content of rice and soybean. *IEEE Geosci. Remote Sensing Lett., 9*, 564–568. https://doi.org/10.1109/LGRS.2011.2174772

Kou, H., Liao, Z., Zhang, H., Lai, Z., Liu, Y., Kong, H., Li, Z., Zhang, F., & Fan, J. (2024). Grain yield, water-land productivity and economic profit responses to row configuration in maize-soybean strip intercropping systems under drip fertigation in arid northwest China. *Agricultural Water Management, 297*, Article 108817. https://doi.org/10.1016/j.agwat.2024.108817

LavagnedOrtigue, O. (ESS) (2023) Land statistics and indicators 2000–2021.

Li, C., Guo, B., Wang, G., Zheng, Y., Liu, Y., & He, W. (2020). NICE: Superpixel segmentation using non-iterative clustering with efficiency. *Applied Sciences, 10*, 4415. https://doi.org/10.3390/app10124415

Li, L., Kong, Q., Wang, P., Xun, L., Wang, L., Xu, L., & Zhao, Z. (2019). Precise identification of maize in the North China Plain based on Sentinel-1A SAR time series data. *International Journal of Remote Sensing,*

*40*, 1996–2013. https://doi.org/10.1080/01431161.2018.1504345

Lin, C., Zhong, L., Song, X.-P., Dong, J., Lobell, D. B., & Jin, Z. (2022). Early- and in-season crop type mapping without current-year ground truth: Generating labels from historical information via a topology-based approach. *Remote Sensing of Environment, 274*, Article 112994. https://doi.org/10.1016/j.rse.2022.112994

Liu, L., Xiao, X., Qin, Y., Wang, J., Xu, X., Hu, Y., & Qiao, Z. (2020). Mapping cropping intensity in China using time series Landsat and Sentinel-2 images and Google Earth Engine. *Remote Sensing of Environment, 239*, Article 111624. https://doi.org/10.1016/j.rse.2019.111624

Mandal, D., Kumar, V., Ratha, D., Dey, S., Bhattacharya, A., Lopez-Sanchez, J. M., McNairn, H., & Rao, Y. S. (2020). Dual polarimetric radar vegetation index for crop growth monitoring using Sentinel-1 SAR data. *Remote Sensing of Environment, 247*, Article 111954. https://doi.org/10.1016/j.rse.2020.111954

Maponya, M. G., Van Niekerk, A., & Mashimbye, Z. E. (2020). Pre-harvest classification of crop types using a Sentinel-2 time-series and machine learning. *Computers and Electronics in Agriculture, 169*, Article 105164. https://doi.org/10.1016/j.compag.2019.105164

Mashaba-Munghemezulu, Z., Chirima, G. J., & Munghemezulu, C. (2021). Delineating smallholder maize farms from Sentinel-1 coupled with Sentinel-2 data using machine learning. *Sustainability, 13*, 4728. https://doi.org/10.3390/su13094728

Moumouris, T., Tsironis, V., Psalta, A., & Karantzalos, K. (2025). Large scale mowing event detection on dense time series data using deep learning methods and knowledge distillation. *International Archives of Photogrammetry, Remote Sensing and Spatial Information Sciences, XLVIII-M–7–2025*, 43–48. https://doi.org/10.5194/isprs-archives-xlviii-m-7-2025-43-2025

Mullissa, A., Vollrath, A., Odongo-Braun, C., Slagter, B., Balling, J., Gou, Y., Gorelick, N., & Reiche, J. (2021). Sentinel-1 SAR backscatter analysis ready data preparation in Google Earth Engine. *Remote Sensing, 13*, 1954. https://doi.org/10.3390/rs13101954

Nash, D. J., Klein, J., Endfield, G. H., Pribyl, K., Adamson, G. C. D., & Grab, S. W. (2019). Narratives of nineteenth century drought in southern Africa in different historical source types. *Climatic Change, 152*, 467–485. https://doi.org/10.1007/s10584-018-2352-6

Ni, R., Zhu, X., Lei, Y., Li, X., Dong, W., Zhang, C., Chen, T., Mburu, D. M., & Hu, C. (2022). Effectiveness of common preprocessing methods of time series for monitoring crop distribution in Kenya. *Agriculture, 12*, 79. https://doi.org/10.3390/agriculture12010079

O'Halloran, T., Obaido, G., Otegbade, B., & Mienye, I. D. (2024). A deep learning approach for Maize Lethal Necrosis and Maize Streak Virus disease detection. *Machine Learning with Applications, 16*, Article 100556. https://doi.org/10.1016/j.mlwa.2024.100556

Ouaadi, N., Chehbouni, A., Ayari, E., Ait Hssaine, B., ElFarkh, J., Le Page, M., Er-Raki, S., & Boone, A. (2025). Root zone soil moisture mapping at very high spatial resolution using radar-derived surface soil moisture product. *Agricultural Water Management, 314*, Article 109507. https://doi.org/10.1016/j.agwat.2025.109507

Pérez-Hoyos, A., Rembold, F., Kerdiles, H., & Gallego, J. (2017). Comparison of global land cover datasets for cropland monitoring. *Remote Sensing, 9*, 1118. https://doi.org/10.3390/rs9111118

Pervez, M. S., & Brown, J. F. (2010). Mapping irrigated lands at 250-m scale by merging MODIS data and National Agricultural Statistics. *Remote Sensing, 2*, 2388–2412. https://doi.org/10.3390/rs2102388

Potapov, P. V., Turubanova, S. A., Hansen, M. C., Adusei, B., Broich, M., Altstatt, A., Mane, L., & Justice, C. O. (2012). Quantifying forest cover loss in Democratic Republic of the Congo, 2000–2010, with Landsat ETM+ data. *Remote Sensing of Environment, 122*, 106–116. https://doi.org/10.1016/j.rse.2011.08.027

Prins, A. J., & Van Niekerk, A. (2021). Crop type mapping using LiDAR, Sentinel-2 and aerial imagery with machine learning algorithms. *Geo-Spatial Information Science, 24*, 215–227. https://doi.org/10.1080/10095020.2020.1782776

Rhein, S., & Jansesberger, V. (2024). Does drought exposure erode trust in the political system in sub-Saharan Africa? *Climatic Change, 177*, 114. https://doi.org/10.1007/s10584-024-03768-5

Sabah, N.U., Zafar, Z., Satti, F.A., Berns, K., Fraz, M M (2024) Enhancing cotton crop mapping in Pakistan: Integrating transfer and active learning with remote sensing technologies, in: 2024 4th International Conference on Digital Futures and Transformative Technologies (ICoDT2). Presented at the 2024 4th International Conference on Digital Futures and Transformative Technologies (ICoDT2), IEEE, Islamabad, Pakistan, pp. 1–8. https://doi.org/10.1109/icodt262145.2024.10740196

Samasse, K., Hanan, N., Tappan, G., & Diallo, Y. (2018). Assessing cropland area in West Africa for agricultural yield analysis. *Remote Sensing, 10*, 1785. https://doi.org/10.3390/rs10111785

Shao, G., Han, W., Zhang, H., Liu, S., Wang, Y., Zhang, L., & Cui, X. (2021). Mapping maize crop coefficient Kc using random forest algorithm based on leaf area index and UAV-based multispectral vegetation indices. *Agricultural Water Management, 252*, Article 106906. https://doi.org/10.1016/j.agwat.2021.106906

Shuai, G., Zhang, J., Basso, B., Pan, Y., Zhu, X., Zhu, S., & Liu, H. (2019). Multi-temporal RADARSAT-2 polarimetric SAR for maize mapping supported by segmentations from high-resolution optical image. *International Journal of Applied Earth Observation and Geoinformation, 74*, 1–15. https://doi.org/10.1016/j.jag.2018.08.021

Tang, F. H. M., Nguyen, T. H., Conchedda, G., Casse, L., Tubiello, F. N., & Maggi, F. (2024). Cropgrids: A global geo-referenced dataset of 173 crops. *Scientific Data, 11*, 413. https://doi.org/10.1038/s41597-024-03247-7

Teluguntla, P., Thenkabail, P. S., Oliphant, A., Xiong, J., Gumma, M. K., Congalton, R. G., Yadav, K., & Huete, A. (2018). A 30-m landsat-derived cropland extent product of Australia and China using random forest machine learning algorithm on Google Earth Engine cloud computing platform. *ISPRS Journal of Photogrammetry and*

*Remote Sensing, 144*, 325–340. https://doi.org/10.1016/j.isprsjprs.2018.07.017

Tubiello, F. N., Conchedda, G., Casse, L., Hao, P., De Santis, G., & Chen, Z. (2023). A new cropland area database by country circa 2020. *Earth System Science Data, 15*, 4997–5015. https://doi.org/10.5194/essd-15-4997-2023

Van Wart, J., Van Bussel, L. G. J., Wolf, J., Licker, R., Grassini, P., Nelson, A., Boogaard, H., Gerber, J., Mueller, N. D., Claessens, L., Van Ittersum, M. K., & Cassman, K. G. (2013). Use of agro-climatic zones to upscale simulated crop yield potential. *Field Crops Research, 143*, 44–55. https://doi.org/10.1016/j.fcr.2012.11.023

Wang, N., & Zhang, Y. (2021). Adaptive and fast image superpixel segmentation approach. *Image and Vision Computing, 116*, Article 104315. https://doi.org/10.1016/j.imavis.2021.104315

Wang, S., Azzari, G., & Lobell, D. B. (2019). Crop type mapping without field-level labels: Random forest transfer and unsupervised clustering techniques. *Remote Sensing of Environment, 222*, 303–317. https://doi.org/10.1016/j.rse.2018.12.026

Wen, Y., Li, X., Mu, H., Zhong, L., Chen, H., Zeng, Y., Miao, S., Su, W., Gong, P., Li, B., & Huang, J. (2022). Mapping corn dynamics using limited but representative samples with adaptive strategies. *ISPRS Journal of Photogrammetry and Remote Sensing, 190*, 252–266. https://doi.org/10.1016/j.isprsjprs.2022.06.012

Xiong, J., Thenkabail, P. S., Gumma, M. K., Teluguntla, P., Poehnelt, J., Congalton, R. G., Yadav, K., & Thau, D. (2017b). Automated cropland mapping of continental Africa using Google Earth Engine cloud computing. *ISPRS Journal of Photogrammetry and Remote Sensing, 126*, 225–244. https://doi.org/10.1016/j.isprsjprs.2017.01.019

Xiong, J., Thenkabail, P. S., Teluguntla, P. G., Oliphant, A., Gumma, M. K., Giri, C., Pyla, V., Dixit, S., & Whitbread, A. M. (2020). Agricultural cropland extent and areas of South Asia derived using Landsat satellite 30-m time-series big-data using random forest machine learning algorithms on the Google Earth Engine cloud. *Giscience & Remote Sensing, 57*, 302–322. https://doi.org/10.1080/15481603.2019.1690780

Xiong, J., Thenkabail, P., Tilton, J., Gumma, M., Teluguntla, P., Oliphant, A., Congalton, R., Yadav, K., & Gorelick, N. (2017a). Nominal 30-m cropland extent map of continental Africa by integrating pixel-based and object-based algorithms using Sentinel-2 and Landsat-8 data on Google Earth Engine. *Remote Sensing, 9*, 1065. https://doi.org/10.3390/rs9101065

Zhang, D., Pan, Y., Zhang, J., Hu, T., Zhao, J., Li, N., & Chen, Q. (2020). A generalized approach based on convolutional neural networks for large area cropland mapping at very high resolution. *Remote Sensing of Environment, 247*, Article 111912. https://doi.org/10.1016/j.rse.2020.111912

Zhang, L., Wang, W., Ma, Q., Hu, Y., Ma, H., & Zhao, Y. (2024). CCropLand30: High-resolution hybrid cropland maps of China created through the synergy of state-of-the-art remote sensing products and the latest national land survey. *Computers and Electronics in Agriculture, 218*, Article 108672. https://doi.org/10.1016/j.compag.2024.108672

Zhang, L., Zhang, L., & Du, B. (2016). Deep learning for remote sensing data: A technical tutorial on the state of the art. *IEEE Geoscience and Remote Sensing Magazine, 4*, 22–40. https://doi.org/10.1109/MGRS.2016.2540798

Zhang, R., An, A., Cen, M., Zhang, C., Huangfu, A., Vinnakota, S., Song, S (2025) FragMangro: A cross-domain zero-shot model for monitoring fragmented mangrove ecosystems. *J King Saud Univ Comput Inf Sci 37*. https://doi.org/10.1007/s44443-025-00053-y